

Skyrme-Hartree-Fock-Bogoliubov mass models on a 3D mesh: IIb. Fission properties of BSkG2.

Wouter Ryssens^{a,1}, Guillaume Scamps^{1,2}, Stephane Goriely¹, Michael Bender³

¹Institut d'Astronomie et d'Astrophysique, Université Libre de Bruxelles, Campus de la Plaine CP 226, 1050 Brussels, Belgium

²Department of Physics, University of Washington, Seattle, Washington 98195-1560, USA

³Université de Lyon, Université Claude Bernard Lyon 1, CNRS / IN2P3, IP2I Lyon, UMR 5822, F-69622, Villeurbanne, France

the date of receipt and acceptance should be inserted later

Abstract Large-scale models of nuclear structure are currently the only way to provide consistent datasets for the many properties of thousands of exotic nuclei that are required by nucleosynthesis simulations. In [W. Ryssens et al., Eur. Phys. J. A **58**, 246 (2022)], we recently presented the new BSkG2 model based on an energy density functional of the Skyrme type. Relying on a flexible three-dimensional coordinate representation of the nucleus, the model takes into account both triaxial deformation and time-reversal symmetry breaking. BSkG2 achieves a state-of-the-art global description of nuclear ground state (g.s.) properties and reproduces in particular the known masses with a root-mean-square (rms) deviation of 678 keV. Moving beyond g.s. properties, the model also reproduces all empirical values for the primary and secondary barriers as well as isomer excitation energies of actinide nuclei with rms deviations below 500 keV, i.e. with unprecedented accuracy. Here we discuss in detail the extension of our framework to the calculation of the fission barriers of 45 actinide nuclei, including odd-mass and odd-odd systems. We focus in particular on the impact of symmetry breaking which is key to the accuracy of the model: we allow systematically for axial, reflection and time-reversal symmetry breaking. The effect of the latter on the fission properties of odd-mass and odd-odd nuclei is small, but we find that allowing for shapes with triaxial or octupole deformation, as well as shapes with *both*, is crucial to achieving this accuracy. The numerical accuracy of our coordinate space approach, the variety of nuclear configurations explored and the simultaneous successful description of fission properties and known masses makes BSkG2 the tool of choice for the large-scale study of nuclear structure.

1 Introduction

Nuclei play a prominent role in astrophysics: their reactions and decays release the energy that powers the light emitted by stars, staving off their eventual collapse for as long as these processes can be maintained. The few hundred species of stable nuclei occurring on Earth can teach us much, but not everything: thousands of short-lived isotopes play a role in the nucleosynthesis of heavy elements and the structure of exotic astrophysical objects such as neutron stars. Understanding these aspects of the Universe requires data on the properties of these nuclei, which can in turn be used to model their reactions and decays. The most demanding application in terms of data requirements is the simulation of the rapid neutron capture process or r-process, a process which produces a sequence of increasingly neutron-rich elements through repeated neutron captures which decay through a variety of channels to produce stable elements heavier than iron [1].

It is impossible to measure all relevant properties of the enormous number of exotic nuclei involved in the r-process, the majority of which have so far not even been synthesised on Earth. The only way to access the required information then is modelling: nuclear theory endeavours to construct large-scale models that can provide reliable extrapolations for neutron-rich nuclei. The focus of this effort is often nuclear binding energies: semi-empirical models, either based on the original work by Von Weizsäcker [2] or that by Duflo and Zuker [3], microscopic-macroscopic ('mic-mac') approaches such as those of Refs. [4–6] and microscopic approaches based on energy density functionals (EDFs) [7–12]. Most of these models reach a root-mean-square (rms) deviation for all nuclear masses that ranges from 500 to 800 keV, though some of the semi-

^ae-mail: wouter.ryssens@ulb.be

empirical formulas can reach 200-300 keV [3]. Machine learning techniques have been used to produce standalone models of nuclear masses [13], but are more often used to augment the other approaches mentioned [14–20]. Although such hybrid approaches can sometimes reach an extremely small rms deviation on the known masses of 100 keV or lower [20], the resulting extrapolations towards neutron-rich nuclei still depend on the underlying model [21].

However, nucleosynthesis simulations require a more complete picture of nuclear structure than just an accurate description of masses; what is needed is a consistent set of all nuclear structure properties needed for reaction and decay calculations. Fission properties for instance, impact several aspects of the r-process such as (i) the details of fission recycling, (ii) the r-process abundances in the $110 \leq A \leq 170$ region, (iii) the production of cosmic chronometers such as Th and U [22, 23] and (iv) the heating rate of kilonovae [24]. The theoretical description of nuclear fission in general and the fission of actinides in particular has a long history [25] and remains today a very active field of research, see e.g. Refs. [26–29] for recent reviews. Nevertheless, the community still faces many challenges [30] and a complete description of fission remains difficult, particularly when aiming at thousands of neutron-rich nuclei. This difficulty partially explains the relative rarity of large-scale fission models when compared to the available mass models. Models that combine an accurate reproduction of masses and fission properties are even more rare: only microscopic-macroscopic approaches [6] and EDF-based models [9, 31, 32] have been successful at describing both simultaneously¹. Of the two, only EDFs offer a consistent microscopic description of the nucleus in terms of its constituent nucleons.

Employing EDFs of the Skyrme type [33], we have recently started the development of the Brussels-Skyrme-on-a-Grid (BSkG) series of models [11, 12] in the spirit of the earlier BSk-models (see Ref. [9] and references therein). The main goal of the BSkG models is providing consistent nuclear data for astrophysical applications that is competitive with more phenomenological approaches, while gradually including additional physical ingredients in a microscopic way. Key to this strategy is the inclusion of thousands of nuclear binding energies in the objective function of the parameter adjustment, which imposes both harsh constraints on the parameter values and requires significant computational effort. Where the BSk-models relied on the

assumption of axial symmetry that reduces the structure of a nucleus to two dimensions, the BSkG-series does away with this restriction and utilises a numerical representation in terms of a three-dimensional coordinate space mesh [34]. In Ref. [11] we employed this representation to fit the parameters of BSkG1 to the masses of thousands of nuclei, all of which were free to exploit triaxial deformation to lower their total energy. For the construction of BSkG2, we also included degrees of freedom that break time-reversal symmetry in the nuclear mean fields: these impact the masses of odd-mass and odd-odd nuclei and several other quantities such as magnetic moments and rotational moments of inertia [12].

Here we extend the reach of the BSkG series to nuclear fission: we study in detail the fission barriers and isomer excitation energies predicted by BSkG2. Unfortunately, a good fit to ground state (g.s.) properties does not imply realistic predictions for barriers, as nuclear ground states exhibit small to moderate deformation while the shapes relevant to fission are typically very elongated [35–37]. For this reason we included in the objective function of the BSkG2 model the RIPL-3 empirical values for the primary and secondary fission barriers of twelve even-even actinide nuclei [38] as well as the fission isomer excitation energies for seven of these. As already discussed briefly in Ref. [12], BSkG2 achieves an unprecedented accuracy for three different fission properties: primary and secondary barrier heights and isomer excitation energies. For the 45 nuclei with $Z \geq 90$ included in the RIPL-3 database [38], the model achieves rms deviations below 500 keV for all three quantities *simultaneously*. This accuracy does not come at the expense of masses: BSkG2 describes the 2457 known binding energies of nuclei with $Z \geq 8$ in AME20 [39] with an rms of 678 keV.

Aside from the lowered rms deviations as compared to earlier models, there are two further points that make BSkG2 uniquely suited to the large-scale description of fission. The first is our use of a coordinate-space representation, which allows us to reach high numerical accuracy even for the extremely elongated shapes associated with nuclear fission [40]. The second is the large diversity of nuclear configurations we consider: we consistently include triaxial deformation in all our fission calculations and, where relevant, combine it with reflection asymmetry and octupole deformation. For the double-humped barriers of actinide nuclei, triaxial deformation can lower both the inner barrier by more than an MeV [33, 41, 42] and the outer barrier by several hundred keV [43–45]. Although we do not study any superheavy nuclei with $Z \gtrsim 110$ here, their fission barriers can be even more strongly affected [46–49]. Despite

¹For microscopic-macroscopic models an accurate description of fission barriers deteriorates the description of the masses, hence why Ref. [6] advocates using two separate models: FRDM for masses and FRLDM for fission.

this, triaxial deformation has up to now been neglected in large-scale studies of fission based on EDFs, likely due to its numerical cost. Furthermore, our treatment of the fission properties of odd-mass and odd-odd nuclei is as advanced as our description of their g.s. properties. Invoking no approximations, we describe such nuclei with blocking calculations that include the effect of the time-odd terms of the EDF, although we will establish below that their effect on barriers and isomer excitation energies is small. To the best of our knowledge, we are the first to report on self-consistent Hartree-Fock-Bogoliubov (HFB) calculations that consider blocking for odd-mass and odd-odd nuclei while breaking axial, reflection and time-reversal symmetry simultaneously.

This paper is organized as follows: we summarize the relevant aspects of the construction of BSkG2 and specify the numerical conditions of the fission calculations in Sec. 2. In Sec. 3 we discuss the fission barriers of ^{232}U , ^{240}Pu and ^{244}Pu as representative examples. We discuss fission properties of nuclei in the actinide region more systematically in Sec. 4 and present our conclusions and outlook in Sec. 5.

2 The BSkG2 model

2.1 Binding energy and collective correction

We define the total binding energy of a nucleus, represented by a state $|\Phi\rangle$ of the HFB type as:

$$E_{\text{tot}} = E_{\text{HFB}} + E_{\text{corr}}. \quad (1)$$

In Eq. (1), E_{HFB} is the self-consistent mean-field energy and E_{corr} is the collective correction energy. The mean-field energy contains the kinetic energy as well as the Skyrme and Coulomb energies that determine, respectively, the strong and electrostatic interaction between the nucleons. The form of the Skyrme EDF we employ is essentially standard, but does include well-defined time-odd terms [12].

The goal of the correction energy is modelling correlations that cannot be captured by a single HFB state built from separate proton and neutron orbitals: rotational and vibrational collective motion, centre-of-mass motion and proton-neutron pairing. These four effects each give rise to a term in the correction energy:

$$E_{\text{corr}} = E_{\text{rot}} + E_{\text{vib}} + E_{\text{cm}}^{(2)} + E_{\text{W}}, \quad (2)$$

where these are, respectively, the rotational and vibrational correction [50, 51], the two-body part of the centre-of-mass correction [52], and the Wigner energy [53].

The rotational and vibrational correction have the same form and are combined as

$$E_{\text{rot}} + E_{\text{vib}} = - \sum_{\mu=x,y,z} (f_{\mu}^{\text{rot}} + f_{\mu}^{\text{vib}}) \frac{\langle \hat{J}_{\mu}^2 \rangle}{2\mathcal{I}_{\mu}}, \quad (3)$$

where \mathcal{I}_{μ} is the Belyaev moment of inertia (MOI) around Cartesian axis μ . The factors $f_{\mu}^{\text{rot/vib}}$ are both defined in terms of $B_{\mu} = \mathcal{I}_{\mu}/\mathcal{I}_c$, the ratio of the Belyaev MOI to that of (one third of) a rigid rotor \mathcal{I}_c [12]:

$$f_{\mu}^{\text{rot}} = b \tanh(cB_{\mu}), \quad (4a)$$

$$f_{\mu}^{\text{vib}} = dB_{\mu} e^{-l(B_{\mu} - B_0)^2}. \quad (4b)$$

As in Ref. [12], we stress that the vibrational component of Eq. (3) only intends to capture the *deformation dependence* of the spurious collective vibrational energy. Since Eq. (3) vanishes for spherical configurations, we put the burden of simulating any collective vibrational energy that is deformation independent on the EDF coupling constants. Expressions for all other ingredients of the total energy can be found in Refs. [11, 12].

2.2 Shapes, fission paths and barriers

Modelling nuclear fission starts with the selection of a set of collective coordinates that characterize the large-scale collective motion of the nucleus on its way to scission. Traditionally, one uses a small number of (mass) multipole moments $Q_{\ell m}$ that characterize the shape of the nucleus. We define the $Q_{\ell m}$ and their dimensionless equivalents $\beta_{\ell m}$ for integer (ℓ, m) with $\ell \geq 1$ and $0 \leq m \leq \ell$ as

$$\langle Q_{\ell m} \rangle = \int d^3r \rho_0(\mathbf{r}) r^{\ell} \Re[Y_{\ell m}(\theta, \phi)], \quad (5a)$$

$$\beta_{\ell m} = \frac{4\pi}{3R^{\ell}A} Q_{\ell m}, \quad (5b)$$

where $R = 1.2A^{1/3}$ fm. Replacing the total density $\rho_0(\mathbf{r})$ in Eq. (5a) by the proton, neutron or charge density and substituting A by the appropriate particle number in the denominator of Eq. (5b), one obtains the deformations $\beta_{\ell m,p}$, $\beta_{\ell m,n}$ or $\beta_{\ell m,c}$, respectively. For plotting purposes, we will also employ the alternate (β, γ) characterization of quadrupole deformation, defined as

$$\beta = \sqrt{\beta_{20}^2 + 2\beta_{22}^2}, \quad (6a)$$

$$\gamma = \text{atan}\left(\sqrt{2}\beta_{22}/\beta_{20}\right). \quad (6b)$$

One of the quadrupole deformations, β_{20} , characterizes the elongation of the nuclear shape in the z -direction

and is virtually always employed as collective coordinate. The octupole deformation, β_{30} , reflects the left-right asymmetry of the nuclear density distribution along the z -axis and is a traditional second choice. The second quadrupole degree of freedom β_{22} [42, 43, 45, 54], the hexadecapole moment β_{40} [55] and the particle number dispersions $\Delta N_q^2 \equiv \langle \hat{N}_q^2 \rangle - \langle \hat{N}_q \rangle^2$ of both nucleon species ($q = p, n$) [54] have all been used as collective coordinates in the study of fission paths.

Once a set of coordinates has been chosen, the goal is to study the movement of the nucleus in this collective space along (continuous) paths that connect the ground state to a configuration of two disconnected nuclei, i.e. a fissioned system. By minimizing an appropriate action integral, one can obtain the trajectory that gives the nucleus the highest probability of tunneling through the barrier(s) in a semiclassical approach [56, 57]: this is the least action path (LAP). The action integral depends on the total energy and the inertial mass tensor associated with the collective coordinates, and the calculation of both in the entire collective space is required in order to be able to minimize the action.

Ideally, one (i) constructs a complete potential energy surface (PES) in all relevant collective degrees of freedom and (ii) minimizes the action among all possible paths. Both of these represent enormous computational challenges if one moves beyond more than a few collective degrees of freedom. This study is an initial step towards more extensive calculations for thousands of nuclei; in view of this computational challenge, we limit ourselves here to two collective degrees of freedom: β_{20} and β_{22} . We do not attempt to construct the LAP, but restrict ourselves to the simpler concept of the least energy path (LEP) [57]. This path can be constructed without calculation of the inertia tensor, and therefore ignores all dynamical aspects of the fission process. The local maxima encountered along the (one-dimensional) LEP are, by construction, saddle points on the complete (multi-dimensional) PES. It is the energies of these saddle points, normalized to the corresponding g.s., that we compare to the empirical values of the RIPL-3 database.

Our calculation of the fission properties of a nucleus thus consists of two steps. First, we explore the relevant part of the collective space with numerous EDF calculations constrained to different values of the collective coordinates (β_{20}, β_{22}). A robust algorithm to adjust the numerical parameters of the quadratic constraints we imposed on these multipole moments greatly simplifies these calculations [34]. The shape degrees of freedom explored by nuclei in our calculations are however *not* restricted to the two quadrupole moments: a self-consistent EDF calculation will employ all multi-

pole moments to optimize the mean-field energy, limited only by symmetries imposed on the calculation by either the numerical implementation or the starting point of the iterative process. In contrast to microscopic-macroscopic approaches where the shape degrees of freedom explored by the nuclei and the collective coordinates are identical, our calculations thus naturally include all multipole moments that our numerical choices allow for, see also Sec. 2.4 and Ref. [12]. More specifically, our calculations allow for non-zero values of the $\beta_{\ell m}$ for arbitrary $\ell > 0$ and even values of m^2 . In particular, this set includes multipole moments with odd ℓ that break reflection symmetry, the most important of which is the octupole moment β_{30} . Octupole deformation is crucial to the description of the fission of actinide nuclei, but the construction of three-dimensional PESes in ($\beta_{20}, \beta_{22}, \beta_{30}$) is still prohibitively expensive for more than a handful of nuclei. Luckily, the topographies of the PESes of the nuclei we consider here are all similar and not too complicated: we will demonstrate in Sec. 3 that the LEPs we construct from two-dimensional PESes are closely equivalent to those we would have obtained from much more computationally expensive three-dimensional PESes.

Not all values of multipole moments correspond to distinct shapes though: the (body-fixed) principal axes of a deformed but reflection-symmetric shape can be assigned to the x -, y - and z -axes in the simulation volume in three different ways. If the configuration is invariant under time-reversal, these three possibilities are all physically equivalent. If the shape is in addition also reflection asymmetric, the number of such equivalent orientations rises to six. When the configuration breaks time-reversal symmetry, all these possibilities are not exactly equivalent any longer since the finite angular momentum determines a preferred direction in space; the energy difference due to a reorientation of the principal axes has never been studied for odd-odd systems but is on the order of 100 keV for heavy odd-mass nuclei [94]. For simplicity, we ignore this reorientation effect entirely as we did in Ref. [12] and limit our calculations to a specific part of the collective space with little loss of generality: $\gamma \in [0, 60]^\circ$ and $\beta_{30} \geq 0$. Finally, the mass dipole ($\ell = 1$) moments are proportional to the center-of-mass of the nucleus and do not represent physical degrees of freedom. Only β_{10} is not restricted by our symmetry choices; we constrain it to be zero in all calculations in order to optimize the placement of the nucleus in the simulation volume.

²As for the g.s. calculations of Ref. [12], we still impose z -signature as self-consistent symmetry which implies that $\beta_{\ell m}$ vanishes if m is odd.

As second step to calculate the fission properties of a nucleus we use a flooding model [57] to determine the LEP; along which we interpolate to obtain the saddle points. We determine fission isomer excitation energies by searching for the local minimum of the PES at moderate deformation, $\beta_{20} \sim 0.9$. This workflow is universally applied to all nuclei. Our treatment of odd-mass and odd-odd nuclei differs from that of even-even nuclei only in the underlying EDF calculations: the PES was constructed from self-consistent calculations with quasiparticle blocking that included the effects of time-reversal symmetry breaking [12]. We stick to the techniques of Ref. [12]: we limit ourselves to quasiparticle excitations with z -signature eigenvalue $\eta = +i$ and use a gradient-based HFB solver to combat convergence issues and guarantee that we obtain the lowest possible energy for each value of (β_{20}, β_{22}) .

Fission paths obtained from self-consistent calculations with a limited number of collective degrees of freedom can be plagued with discontinuities [58]. In this sense, our search for the LEP is crude: we made no attempt to explicitly check that the paths we obtain are continuous. Visual inspection of our results did not reveal obvious signs of discontinuities, such as large jumps in the total energy or any multipole moment from one point on the fission path to the next. It is not excluded that the LEPs we obtain are affected by more subtle discontinuities, but it is not easy to identify such problems and even harder to cure them if found. We interpret the apparent absence of discontinuities as due to the inclusion of triaxial deformation. Most calculations of fission barriers that can be found in the literature restrict the nucleus to axial symmetry which separates all single-particle states into symmetry blocks determined by the K quantum number. Triaxial deformation allows the nucleus to connect these symmetry blocks in a continuous way, drastically reducing the possibility for discontinuous changes in single-particle configuration from one calculated point on the PES to the next as compared to axially symmetric calculations.

The situation is more complicated for odd-mass and odd-odd nuclei: the properties of the blocked quasiparticle(s) can vary dramatically for even small changes in deformation, introducing in this way a possible second source of discontinuities. As in previous studies [35], we simply take the overall lowest energy at any grid point on the PES and thus pass over any consideration of conserved quantum numbers when establishing the LEP. Anticipating that we will find that all nuclei studied here will take triaxial shapes at all relevant saddle points for the LEP, our choice can be motivated by the inevitable mixing of quasiparticles with different K quantum numbers when the fission path

passes through triaxial shapes, and the mixing of quasiparticles with different parity when passing through octupole-deformed shapes. In particular around the outer saddle point, z -signature is the only remaining quantum number of the single-particle states. All quasiparticles we consider for blocking purposes have z -signature $\eta = +i$, such that in this region of the path our calculations cannot encounter any level crossings that could introduce discontinuities.

Because the treatment of blocked quasiparticles adds significant complexity to a calculation, fission barriers for odd-mass and odd-odd nuclei are rarely considered in the literature, with notable exceptions being Refs. [60–63] and [64]. All of these studies are limited to a few nuclei only, and all limit the possible shapes to axial ones. The authors of these references also do not construct configurations with the lowest energy at each point of the collective space, but rather construct paths at fixed K quantum number in order to reduce the occurrence of discontinuities encountered. The large-scale fission calculations with BSk14 of Ref. [35] form an exception: while restricted to axial symmetry, the authors did not enforce constant K along the fission path, likely leading to large numbers of discontinuities. The question how to construct a consistent fission path in completely symmetry-unrestricted calculations will require further investigation in the future [30], particularly when attempting the description of more complex observables such as lifetimes or fission yields.

2.3 Parameter adjustment and global performance

The total binding energy E_{tot} depends on 25 parameters that were adjusted to experimental data. We reported the BSkG2 parameter values in Ref. [12] and discussed there the parameter adjustment and the performance of the model for g.s. properties. Here, we summarize only a few key points.

The main ingredient of the objective function is the ensemble of 2457 measured binding energies ($Z \geq 8$) tabulated in the AME20 database [39]. We also constrained the EDF parameters so that the calculated uv -averaged neutron pairing gaps $\langle \Delta \rangle_n$ [65] reproduce as best as possible the experimental five-point gaps $\Delta_n^{(5)}$ in order to obtain a realistic pairing strength for the neutrons. The fit included constraints on the models infinite nuclear matter properties, such as the symmetry energy ($J \in [30, 32]$ MeV) the nuclear incompressibility ($K_\nu \in [230, 250]$ MeV and the isoscalar effective mass $M_s^*/M \approx 0.84$). Finally, we adjusted the Fermi wave number k_F to reproduce 884 measured charge radii [66].

The selection of g.s. properties is close to those that figured in the objective function of BSkG1. For BSkG2, we also included empirical values for the primary (E_I) and secondary (E_{II}) fission barriers of twelve even-even nuclei with $92 \leq Z \leq 96$ from RIPL-3 [38] and their fission isomer excitation energies (E_{iso}) when available [67]. As already explained in Ref. [12], we did not employ all nuclei included in the RIPL-3 database in order to (i) focus on nuclei with low fission barriers ($E_I < 10$ MeV) due to their relevance to r-process nucleosynthesis and (ii) not to further complicate the adjustment process with the fission barriers of odd-mass and odd-odd nuclei. Our final selection of twelve primary and secondary barrier heights and seven isomer excitation energies is summarised in Table 1. These empirical values are certainly not without associated uncertainties. The fission barriers themselves are at best pseudo-observables, quantities that can only be extracted in a model dependent way. We are not aware of any attempt to quantify the uncertainties of the RIPL-3 recommended values. Although isomer excitation energies are directly observable, their accurate measurement remains difficult: for example, the literature reports values for the isomer excitation energy of ^{240}Pu that range from 2.25 ± 0.2 MeV [68] to ≈ 2.8 MeV [69]. This uncertainty also extends to the quantum numbers of the fission isomers: their spin and parity are not guaranteed to be identical to those of the ground state. Except for the fission isomer of ^{238}U [70], only a handful of tentative spin-parity assignments are available [69].

Two remarks on nomenclature are in order. First, we will follow much of the literature in using the word ‘barrier’ as a shorthand for ‘excitation energy of the saddle point’ to describe our results if the context permits us to do so. Second, for the double-humped fission barrier of actinide nuclei it is natural to discuss ‘inner’ and ‘outer’ barriers that correspond to the saddle points encountered along the LEP at moderate and large elongation, respectively. ‘Primary barrier’ and ‘secondary barrier’ then refer to the saddle points located at highest and lowest excitation energy compared to the g.s. minimum, respectively. The RIPL-3 database lists reference values for inner and outer barriers as deduced from fits to experimental fission cross sections. However, the fission transmission coefficients employed in such fits are not sensitive to the ordering of saddle points, only to their excitation energies [38]. For this reason, our comparisons with empirical values in the objective function of the parameter adjustment and in the text below always concern primary and secondary barriers, *not* inner and outer barriers.

As explained in Sec. 2.2, obtaining the fission path of even a single nucleus is a computationally demand-

Z	A	E_I	E_{II}	E_{iso}
92	232	5.40	4.90	-
92	234	5.50	4.80	-
92	236	5.67	5.00	2.30
92	238	6.30	5.50	2.60
94	238	5.60	5.10	2.40
94	240	6.05	5.45	2.25
94	242	5.85	5.05	-
94	244	5.70	4.85	2.00
96	242	6.65	5.00	1.80
96	244	6.18	5.10	1.04
96	246	6.00	4.80	-
96	248	5.80	4.80	-

Table 1 Values for the primary (E_I) and secondary (E_{II}) fission barriers as well as the isomer excitation energies E_{iso} included in the parameter adjustment. Barrier values are the empirical values recommended in Ref. [38], isomer excitation energies are those of Ref. [67]. All energies are expressed in MeV.

ing and complex multi-step procedure that is difficult to automate consistently. This means that the practical inclusion of barriers in the objective function is extremely challenging and, to the best of our knowledge, has never been achieved for an EDF-based model before. Instead, simplifications have been adopted: the adjustment of the early SkM* Skyrme parameterization employed semiclassical estimates of the barrier of ^{240}Pu [71], the surface coefficient of the Gogny D1S parameterization was manually changed to reproduce the barrier of ^{240}Pu [72] and the UNEDF1 and UNEDF2 parameterizations used four fission isomer excitation energies instead of barriers in the adjustment protocol [73, 74]. The authors of Ref. [37] constructed a series of parameter sets with systematically varied values of the surface energy coefficient, of which SLy5s1 is the one that best describes the excitation energy of superdeformed states and fission barriers [37, 44]. The BSk14 parameterization was created in two steps: an initial fit to g.s. properties, followed by the fine-tuning of the (few) parameters characterizing the collective correction to fission barriers [35].

For BSkG2, we adopted a two-step adjustment procedure identical to that used for BSk14 [35]. First, we adjusted all parameters of the EDF to the g.s. properties included in the objective function. Using the intermediate parameter values issuing from this step, we calculated the PESes for the twelve even-even nuclei in Tab. 1. Freezing all other parameters, we then adjusted the nine parameters of the collective correction ($V_W, \lambda, V'_W, A_0, b, c, d, l$ and β_{vib}) to the complete objective function including fission properties, g.s. properties and masses. Since the collective correction is treated semi-variationally, the changes induced in the PESes

(and therefore the saddle points) by the variation of these parameters can be obtained at essentially no computational cost with the values of $\langle \hat{J}_{x/y/z}^2 \rangle$ and $\mathcal{I}_{x/y/z}$ tabulated in the first step. We thus eliminated the need for the repeated construction of complete PESes, although we continued EDF calculations for the g.s. properties of nuclei during the second step.

As already pointed out in [12], this simple procedure for adjusting the barrier heights through a fine-tuning of the correction energy is sufficient because the fit to masses already provides quite realistic surface properties in the first step, with barriers typically deviating by less than 2 MeV from the empirical values. If the parameters issued from the first step yielded fission barriers that are too high by 10 MeV as is the case for many Skyrme EDFs [37], this could not be corrected for by a small modification of a correction whose variation between ground state and saddle points is typically on the order of 2 MeV, as we will illustrate in Sec. 3. One of the keys to finding reasonable agreement for fission barriers without including them in the objective function is the inclusion of the two-body part of the centre-of-mass correction in the EDF [52, 75], as we do here.

The resulting BSkG2 model achieves an rms deviation on the known nuclear masses of $\sigma(M) = 0.678$ MeV, and an rms deviation on the nuclear charge radii of $\sigma(R_c) = 0.0274$ fm, while offering reasonable predictions for the empirical properties of infinite nuclear matter [12]. The performance of the model with respect to the AME20 masses is slightly better than that of BSkG1, which has $\sigma(M) = 0.734$ MeV [11]. It is however worse than the later entries in the BSk series that have rms deviations somewhat below 0.6 MeV [9]. Nevertheless, BSkG2 does significantly better than other Skyrme models: they often reach rms deviations of more than two MeV [76, 77] as their fit protocol typically includes only the binding energies of a handful of nuclei.

We reported already in Ref. [12] on the performance of the model on the fission properties of all 45 nuclei with $90 \leq Z$ in the RIPL-3 data base [38], which reach up to $Z = 96$. BSkG2 reproduces both the primary and secondary barrier heights with high accuracy: the rms deviations are 0.44 MeV and 0.47 MeV, respectively. This accuracy is comparable to that achieved for 28 isomer excitation energies, which are described with an rms deviation of 0.49 MeV. Anticipating a more detailed comparison with other models in Sec. 4.4, we already mention here that this degree of accuracy for all three fission quantities is unrivalled in the existing literature.

2.4 Numerical representation and symmetries

As in Refs. [11, 12], we use the MOCCa code for all EDF calculations [34]. It iterates N_N neutron and N_Z proton single-particle wave functions on a cubic three-dimensional Cartesian Lagrange mesh characterized by three numbers of discretisation points N_x, N_y, N_z and a grid spacing dx [78]. This coordinate representation is particularly well suited to the description of fission: it offers a numerical accuracy independent of the nuclear shape [40]. The extremely elongated shapes relevant to fission can be accurately represented, with the only proviso that the simulation volume be sufficiently large.

We impose z -signature and y -time-simplex symmetries on the nuclear configuration for all calculations reported on here, allowing us to reduce the effective number of mesh points in x and y -directions in the calculations by half [34]. In regions of the PES where this lowered the total energy, we allow for octupole deformation by breaking reflection symmetry. This requires the explicit numerical representation of all mesh points in the z -direction but also an additional constraint to ensure the z -coordinate of the nuclear centre-of-mass, or equivalently β_{10} , vanishes at convergence.

For even-even nuclei, we imposed time-reversal symmetry such that we could restrict practical calculations to $(N_N + N_Z)/2$ single-particle wave functions. For odd-mass and odd-odd nuclei, we account for the effects of time-reversal symmetry breaking and explicitly represent all $N_N + N_Z$ single-particle states. As for the calculation of g.s. properties [12], we limit ourselves to quasiparticle excitations with z -signature $\eta = +i$ as mentioned in the previous section.

The most demanding calculations we report on here are those for odd-mass and odd-odd nuclei in regions of the PES where octupole deformation is relevant: elongated shapes require extended meshes and neither reflection nor time-reversal symmetry could be employed to simplify the calculations. To efficiently fit such calculations in the memory of the CPUs available to us, we employed a mesh with $N_z = 40$ and $N_x = N_y = 32$ points at $dx = 0.8$ fm. This mesh is somewhat extended in the z -direction and reduced in the x and y directions as compared to our ground state calculations ($N_x = N_y = N_z = 36$). We used a limited number of single-particle states in the calculations: $N_N = 440$ neutron states and $N_Z = 260$ proton states, independently of the nucleus considered. While these choices somewhat limit the numerical accuracy of our calculation of the *absolute* energy as a function of deformation, we checked that the numerical error of any energy *difference* is generally comparable to the error due to the mesh spacing, i. e. about 100 keV [40]. Furthermore,

the outer barrier for actinide nuclei is typically located at $\beta_{20} \sim 1.3$, i. e. at large, but not extreme, elongation of the nucleus.

3 Topography of an actinide fission barrier

The PESes of the forty-five actinide nuclei we consider have comparable topographies, which we will show explicitly in Sec. 4. Before discussing their systematics, we start here by discussing the typical features of PESes in this region of the nuclear chart using the example of five isotopes that span nearly the entire range of Z and N of the empirical barriers: ^{232}U , ^{236}Np , ^{244}Pu , ^{249}Cm and ^{240}Pu . We will discuss the latter in more detail as it is regularly used as benchmark for fission studies [33, 35, 37, 42, 49, 71, 72, 79–87]. The complete PESes of all five isotopes as a function of β_{20} and $\sqrt{2}\beta_{22}$ are shown in Fig. 1, with the LEP for each indicated by black circles. Axially symmetric (AS) prolate configurations correspond to points on the horizontal axes, while AS oblate configurations lie on the $\gamma = 60^\circ$ lines. The five PESes show similar features such as a well-deformed AS prolate ground state near $\beta_{20} \sim 0.3$ and a second AS minimum near $\beta_{20} \sim 0.9$ that is more than 2.5 MeV above the less deformed minimum. Beyond the range of β_{20} covered by the figure, the energy slopes smoothly down until the scission point is reached, i.e. the deformation at which the nucleus breaks apart into two fragments. Three local maxima are visible in each panel: aside from the spherical point, one (inner) peak at $\beta_{20} \sim 0.55$ and another (outer) near $\beta_{20} \sim 1.3$ separate the g.s. and the isomeric state from scission configurations. For deformations larger than those of the isomer, actinide nuclei prefer reflection asymmetric shapes, characterized by an octupole moment which grows with increasing elongation. Since this shape evolution cannot be deduced from the two-dimensional representation in the top panels of Fig. 1, we provide a more intuitive picture of the elongation of the nucleus through the contour plots of the density of AS prolate configurations of ^{240}Pu in the bottom panel of the figure. In all panels the region at large β_{20} and β_{22} is somewhat irregular: here (at least) two different valleys become close in energy. Since they are located at high excitation energy, we made no effort to completely resolve them.

If one restricts the nucleus to axial symmetry, the corresponding least-energy fission path lies along the horizontal axis in Fig. 1. We will call this path the axially symmetric path (ASP) in what follows. The two saddle points along this path are the tops of the inner and outer peak, which respectively can reach heights of

slightly more than 8 MeV and up to 7 MeV. When allowing for triaxial deformation however, the LEP in the full collective space can detour along both peaks: compared to the ASP, the inner saddle point is lowered by more than an MeV while the effect for the outer saddle point accounts for a few hundred keV. These detours do not take the nuclei very far from the ASP: β_{22} remains small compared to β_{20} and γ remains below 15° in the vicinity of the inner peak and even below 5° beyond $\beta_{20} = 1$. Significant parts of the LEP overlap with the ASP: near the ground state, the superdeformed minimum and beyond the outer saddle point the nucleus prefers AS shapes. As an illustration of the triaxial and reflection-asymmetric configurations encountered near the outer saddle point, we show a three-dimensional isodensity surface for ^{240}Pu in Fig. 2. To underline the three-dimensional nature of this shape, we also provide two-dimensional contour plots of the density in each direction: no two of them are identical.

The nuclei ^{236}Np and ^{249}Cm in Fig. 1 serve as illustrations of the PES of odd-odd and odd-mass nuclei, respectively. They do not appear qualitatively different from those of the even-even nuclei: we have been able to properly converge our self-consistent blocked calculations in all regions of the collective space shown, yet we remind the reader that the evolution of the blocked quasiparticles along the PES can be quite complicated.

While the general features of the PESes are the same for all five nuclei, differences are clearly visible. First, the deformations of ground state and fission isomers grow with increasing neutron number. Second, the height of the inner peak increases with neutron number: from about 6 MeV for ^{232}U to just over 8.8 MeV for ^{249}Cm . The outer peak varies by less: 5.8 MeV for ^{232}U to 5.1 MeV for ^{249}Cm . While the (β_{20}, β_{22}) coordinates of the LEPs in Fig. 1 look qualitatively similar in all cases, the impact of triaxial deformation on the total energy along these paths varies strongly with N : for ^{232}U , triaxial deformation lowers the inner barrier by about an MeV while the effect for ^{249}Cm is close to four MeV. Triaxial deformation also affects the outer barrier more strongly as N increases, although this is not easily visible on Fig. 1. The impact of triaxial deformation on the barriers is sufficiently large to change their evolution with N : among these five isotopes, ^{249}Cm has the largest inner barrier among these five nuclei when restricted to axial symmetry, but if we include β_{22} as collective coordinate its barrier becomes the lowest one.

We will study barriers, isomer excitation energies and their evolution with particle number in a more systematic fashion in Sec. 4.2. For further illustrations, we restrict our attention for now to ^{240}Pu and study its ASP and LEP in more detail in Fig. 3; the top panel

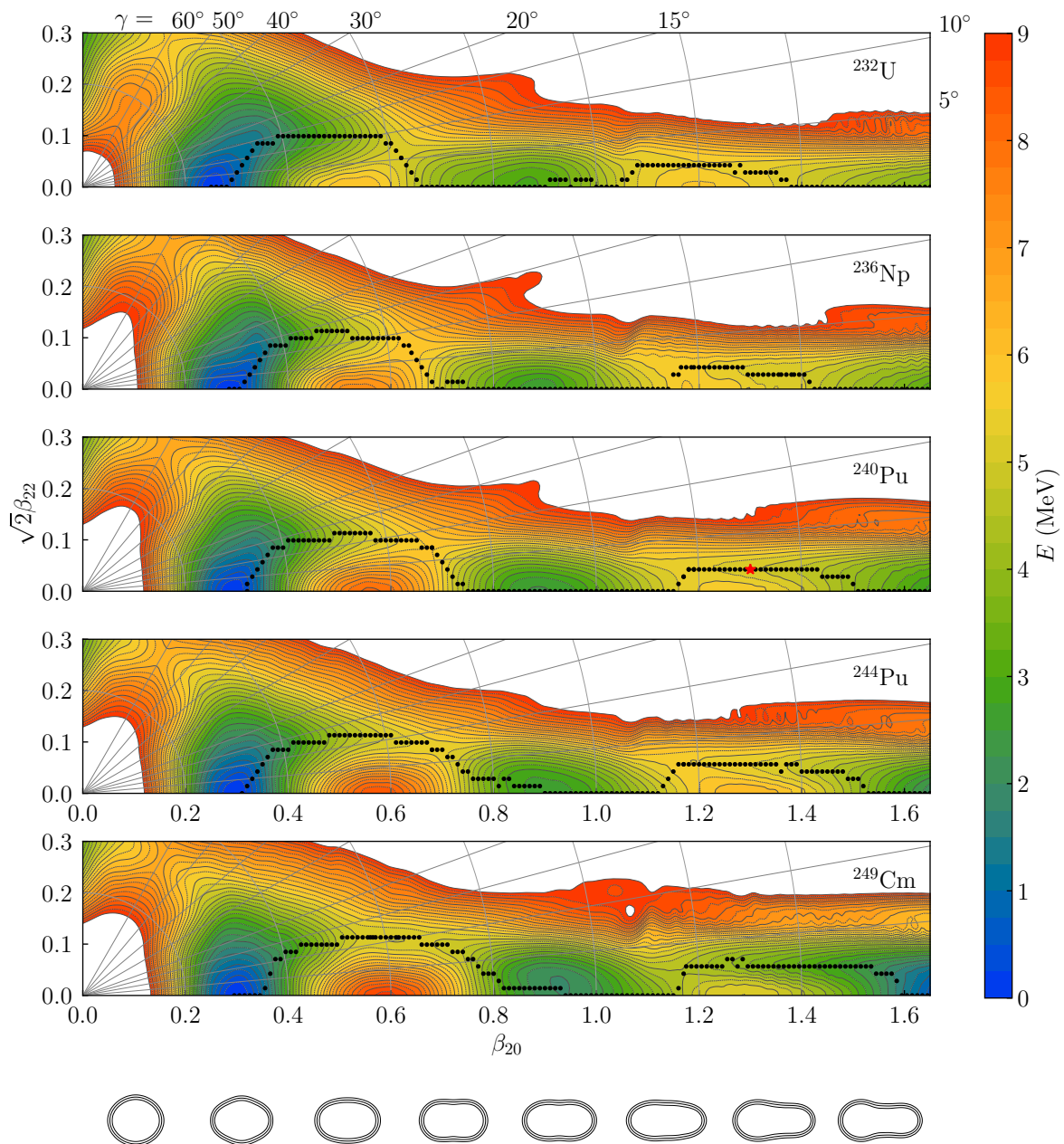


Fig. 1 (Color online) Potential energy surfaces as a function of quadrupole deformation β_{20} and $\sqrt{2}\beta_{22}$ for five nuclei. From top to bottom: ^{232}U , ^{236}Np , ^{240}Pu , ^{244}Pu and ^{249}Cm . All energies are normalized to the g.s. minima near $\beta_{20} = 0.3$. Circles of constant total deformation β and lines of constant γ are drawn in grey. Black circles indicate the lowest energy fission path (see text). Contour lines in the five top panels are 0.25 MeV apart. An indication of the elongation and reflection asymmetry along the surface is given by the contour plots of the total density of axially symmetric configurations of ^{240}Pu for $\beta_{20} = 0.1, 0.3, \dots, 1.5$ (and $\beta_{22} = 0$) below the five panels. The red star in the middle panel indicates the location of the configuration drawn in Fig. 2.

shows the evolution of the total energy along the LEPs and ASPs (full and dashed lines, respectively) obtained with BSkG1 and BSkG2 (black and red lines, respectively), normalized to their respective g.s. minima. The RIPL-3 empirical values for the barrier heights and the isomer excitation energy from Tab. 1 [38, 67] are shown by blue lines at illustrative ranges of β_{20} . The impact

of triaxiality on both barriers can clearly be seen: for BSkG1, including this degree of freedom lowers the inner and outer barrier by about 2.6 MeV and about 120 keV respectively. For BSkG2, the effect on the inner barrier is smaller while that on the outer barrier is larger: they get lowered by about 2.3 MeV and 350 keV, respectively. The impact of triaxial deformation

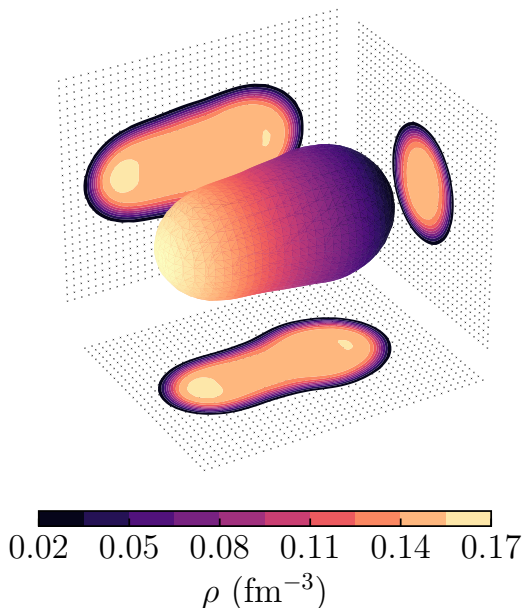


Fig. 2 Isodensity ($\rho = 0.02 \text{ fm}^{-3}$) surface of ^{240}Pu at $\beta_{20} = 1.3$, $\beta_{22} = 0.03$, indicated by the red star in Fig. 1. Two-dimensional contour plots of the total density at $x = 0$, $y = 0$ and $z = 0$ are also shown. The colors of the 3D figure serve only to emphasize the reflection asymmetry of the shape; the color bar refers exclusively to the 2D projections.

we obtain here is somewhat larger than that reported for the SLy5sX-family of Skyrme parameterizations in Ref. [87]: for these, triaxial deformation lowers the inner and outer barrier of ^{240}Pu by about 1.5 MeV and 300 keV, respectively. The barriers and isomer excitation energy obtained with BSkG1 along the LEP match the reference values of Tab. 1 within about an MeV. Although this level of agreement is already quite good, the BSkG2 results are much closer to the empirical values.

The other panels of Fig. 3 show multipole moments other than β_{20} along the LEPs obtained: from top to bottom β_{22} , β_{30} and β_{40} . While we do not show multipole moments such as β_{32} or β_{60} , we remind the reader that these do not vanish and are naturally included in the self-consistent solution procedure. We take the smooth evolution of multipole moments, both those included in Fig. 3 and those that are not, as an indication that the LEPs constructed present continuous trajectories. The sequence of shapes of the nuclear density along the path is robust, at least for this nucleus: β_{30} and β_{40} do not change when either exchanging BSkG1 for BSkG2 or the ASP for the LEP. Octupole deformation vanishes at small to moderate deformations and only beyond $\beta_{20} \sim 1.0$ does the LEP explore reflection-asymmetric shapes. The second quadrupole moment β_{22} remains small along the LEP for both models when compared to β_{20} . While the excitation energies of the saddle points along the fission path are lowered signif-

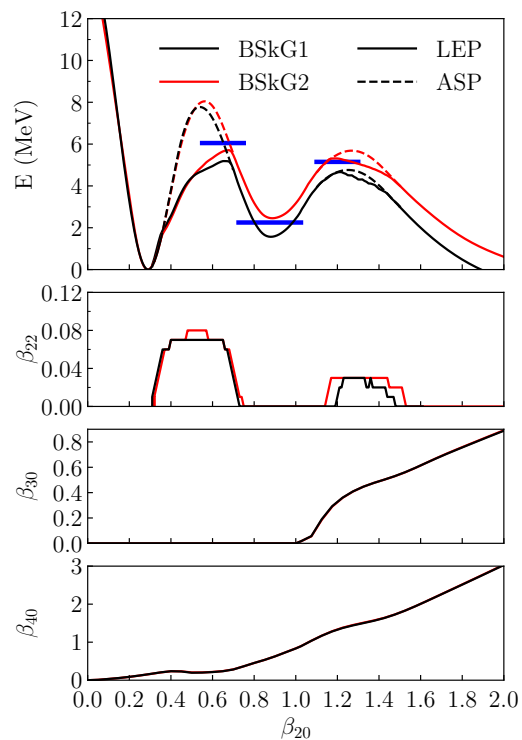


Fig. 3 (Color online) Top panel: Energy of ^{240}Pu along the LEP (solid lines) and ASP (dashed lines) as a function of β_{20} , obtained with BSkG1 (black lines) and BSkG2 (red lines), normalized to the g.s. energies obtained with the respective models. We also show empirical values for the primary and secondary barrier, as well as the isomer excitation energy, drawn at illustrative ranges of β_{20} (blue lines). Second, third and fourth panels: β_{22} , β_{30} and β_{40} along the BSkG1 and BSkG2 LEPs. The octupole and hexadecapole moments of the nucleus along the ASPs are indistinguishable from those along the LEPs and are not shown.

icantly by the inclusion of β_{22} as collective coordinate, the shape evolution of the nucleus as measured by any other multipole moment is essentially unmodified.

In passing, we note that both BSkG1 and BSkG2 reproduce the experimental information on the quadrupole and hexadecapole deformation of the g.s. of ^{240}Pu . We calculate $\beta_{20,c} = 0.287$, $\beta_{40,c} \sim 0.15$ with no difference between models and in excellent agreement with $\beta_{20,c} = 0.293(2)$, $\beta_{40,c} = 0.16(4)$ of Ref. [88] and $\beta_{20,c} = 0.292(2)$, $\beta_{40,c} = 0.151(8)$ of Ref. [89] as determined from Coulomb excitation and the analysis of muonic X rays, respectively³.

³We note that the tables of Ref. [88] and [89] report on deformation parameters that characterize the *surface* of the nuclear shape. These are not equal to our $\beta_{\ell m,c}$, which characterize the shape of the nuclear *volume*, see the discussion in Refs. [87, 90] and references therein. For this reason, the experimental values for the $\beta_{\ell m,c}$ quoted in the text are charge multipole deformations that we consistently calculated from the electric transition moments [91] that are also provided by these references.

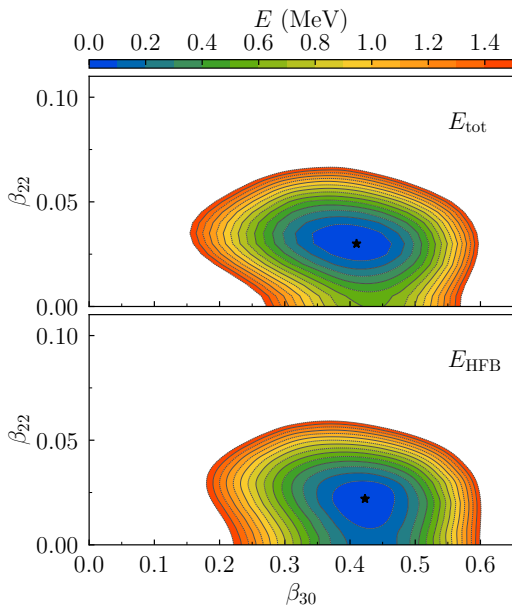


Fig. 4 (Color online) The total energy E_{tot} (top panel) and the mean-field energy E_{HFB} (bottom panel) of ^{240}Pu at (fixed) elongation $\beta_{20} = 1.30$, normalized to their respective minima, as a function of β_{22} and β_{30} . Respective minima are indicated by black stars and contour lines are 100 keV apart.

Next, we illustrate the effect of octupole deformation on the PES and the fission path at large deformation. Fig. 4 shows the total energy (top panel) and the mean-field energy (bottom panel) of ^{240}Pu obtained with BSkG2 as a function of β_{22} and β_{30} at a fixed elongation $\beta_{20} = 1.3$. The minima of both surfaces are situated at almost identical octupole deformation, leading us to two conclusions. First, a hypothetical LEP constructed from a three-dimensional PES using β_{30} as additional collective coordinate would have been close to the one we obtain from our two-dimensional calculations, as would the barriers deduced from it. Second, Fig. 4 illustrates that the preference of the LEP for triaxial deformation is not *only* due to the presence of the collective correction. For this nucleus, the minimum of the uncorrected mean-field energy is not axially symmetric. The inclusion of E_{corr} moves the LEP to a slightly larger value of β_{22} and enlarges the energy difference between triaxial and AS configurations, stabilizing the triaxial deformation when the energy surface is soft in β_{22} .

To illustrate the influence of the collective correction on the PES, we show its evolution along the ASP and LEP in the top panel of Fig. 5 for the BSkG2 model. The contributions of the vibrational and rotational correction along each path are plotted separately in the middle panel. The rotational correction contributes several MeV to the binding energy, except

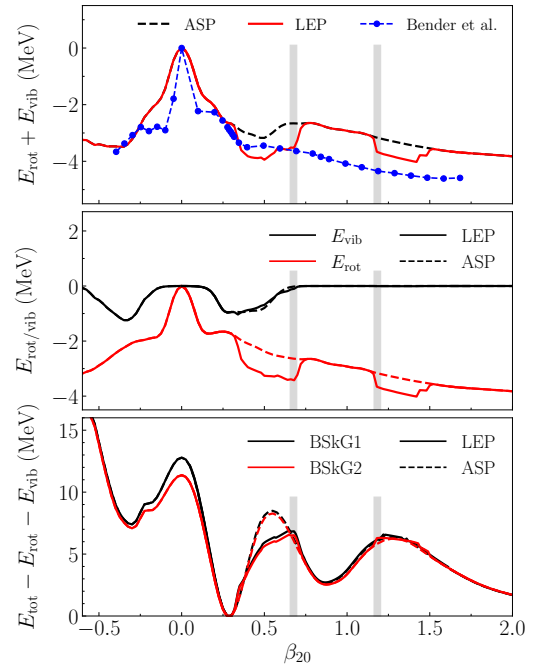


Fig. 5 (Color online) Illustration of the effect of the rotational and vibrational correction for ^{240}Pu . Top panel: the total collective correction for BSkG2 along the LEP (red full line) and along the ASP (black dashed line), compared to the correlation energy obtained by projection on angular momentum $J = 0$ in Ref. [92], using the SLy6 parametrisation of Skyrme's EDF (blue circles). Middle panel: vibrational energy (black curves) and rotational energy (red curves) for BSkG2 along the LEP (full lines) and the ASP (dashed lines). Bottom panel: total energy minus the vibrational and rotational energy for BSkG1 (black curves) and BSkG2 (red curves) along the respective LEPs (full lines) and ASPs (dashed lines). Note that the LEP is obtained from the *total energy*. Faint grey bars are centered on the β_{20} value of the inner and outer saddle points along the LEP with a width of $\delta\beta_{20} = \pm 0.02$.

near the spherical point. Along the ASP the size of this correction increases smoothly with deformation; where the LEP passes through finite values of β_{22} there is an extra contribution on the order of 1 MeV that is associated with the extra rotational degree of freedom. Along both paths, the rotational correction systematically *decreases* both the barriers and the isomer excitation energies. In general, this correction affects more the features of the PES at large deformation. The vibrational correction on the other hand only contributes to the energy for modest deformations $0.1 \lesssim \beta_{20} \lesssim 0.55$: it vanishes near the isomer and the outer saddle point and contributes less than 100 keV near the inner saddle point on the LEP. Because this correction increases the binding energy of the g.s., its presence indirectly *raises* both barriers and the isomer excitation energy in a uniform way.

For comparison with Fig. 3 we show the total energy without both corrections in the bottom panel of

Fig. 5 for both BSkG1 and BSkG2: except at small deformation, the evolution of the energy with deformation for both models is nearly identical⁴. This is supported by Hartree-Fock calculations of semi-infinite nuclear matter along the lines of Ref. [37]: for both models we obtain essentially identical values of the surface energy coefficient $a_{\text{surf}}^{(\text{HF})} = 17.9$ MeV. This is somewhat larger than the value for the SLy5s1 parameterization, $a_{\text{surf}}^{(\text{HF})} = 17.55$ MeV, which was found to be close to optimal for the description of fission properties in Ref. [87] when not including a rotational correction. This difference illustrates the impossibility to establish a unique model-independent empirical value for $a_{\text{surf}}^{(\text{HF})}$: the rotational correction characterises the many-body state and grows with deformation and thereby contributes to the deformation energy. But the rotational correction does not contribute to the surface energy coefficient $a_{\text{surf}}^{(\text{HF})}$, which is a state-independent characteristic of the effective interaction that quantifies the energy loss from the presence of a surface. Hence, when fission properties are included in the parameter fit, models without quantal corrections will have a lower surface energy than models that include such corrections.

The total collective correction we employ here qualitatively agrees with the correlation energy obtained through rotational symmetry restoration for AS configurations of ^{240}Pu using the SLy4 parameterization in Ref. [92], shown by blue circles in the top panel of Fig. 5. The comparison is far from perfect, particularly at large deformation, but firm conclusions are hard to draw due to the differences between conditions of the calculations. In any case, the phenomenological treatment of collective motion remains a weak point of our approach that will require improvement in the future.

4 Actinide fission barriers with BSkG2

4.1 Global description of barriers and isomers

In this section we embark on a more systematic description of the fission properties of 45 $Z \geq 90$ nuclei in the RIPL-3 database: 14 are even-even and 8 are odd-odd, while among the 23 odd-mass systems there are 6 odd- Z and 17 odd- N nuclei. For 28 nuclei among this set⁵, Ref. [67] lists a value for the excitation energy of the isomer: 8 are for even-even nuclei, 4 for odd-odd nuclei

⁴The total energy, on which the construction of the LEP is based, is a smooth function as seen on the top panel of Fig. 3. Its decomposition is not: the discrete steps in β_{22} of the LEP are visible in the non-smooth parts of the LEP curves in Fig. 5.

⁵Ref. [67] lists in fact 30 isomer excitation energies, but we drop for simplicity the values for ^{235}Pu and ^{244}Bk for which RIPL-3 lists no empirical barriers.

		BSkG1			BSkG2	
		M	σ	$\bar{\epsilon}$	σ	$\bar{\epsilon}$
Even-even	E_{I}	14	0.94	+0.90	0.45	+0.31
	E_{II}	14	0.83	+0.67	0.46	+0.01
	E_{iso}	8	0.63	+0.52	0.53	-0.38
Odd- Z	E_{I}	6	0.66	+0.52	0.41	-0.03
	E_{II}	6	0.69	+0.62	0.28	+0.10
	E_{iso}	4	0.66	+0.62	0.40	-0.29
Odd- N	E_{I}	17	0.96	+0.87	0.5	+0.34
	E_{II}	17	0.93	+0.72	0.55	+0.12
	E_{iso}	12	1.35	+0.85	0.46	-0.35
Odd-odd	E_{I}	8	0.73	+0.67	0.28	+0.13
	E_{II}	8	0.95	+0.84	0.43	+0.24
	E_{iso}	4	0.62	+0.50	0.57	-0.43
Total	E_{I}	45	0.88	+0.80	0.44	+0.24
	E_{II}	45	0.87	+0.71	0.47	+0.10
	E_{iso}	28	1.00	+0.67	0.49	-0.36

Table 2 Rms $\sigma(O)$ and mean deviations $\bar{\epsilon}(O)$ of the BSkG1 and BSkG2 models, with respect to RIPL-3 reference values for the primary and secondary barriers [38] and isomer excitation energies from Ref. [67] for different subsets of nuclei: even-even nuclei, odd-mass nuclei with odd Z , odd-mass nuclei with odd N and odd-odd nuclei. M indicates the number of empirical values available for each subset. All energies are expressed in MeV.

and 16 concern odd-mass isotopes. Of the latter, 4 and 12 values are given for odd- Z and odd- N isotopes.

To quantify the performance of BSkG1 and BSkG2 as well as other models in the literature, we will investigate their rms and mean deviations, $\sigma(O)$ and $\bar{\epsilon}(O)$, for three quantities $O = E_{\text{I}}$, E_{II} and E_{iso} , that are the primary and secondary barriers and the excitation energy of the fission isomer as introduced in Sec. 2.3. To avoid confusion about signs, we define the mean deviation of a quantity for which we have access to M empirical and calculated values as:

$$\bar{\epsilon}(O) = \frac{1}{M} \sum_{i=1}^M (O_i^{\text{emp}} - O_i^{\text{th}}). \quad (7)$$

Using this convention, positive (negative) values of $\bar{\epsilon}(O)$ mean that our calculations underestimate (overestimate) the empirical values.

The values of these deviations for BSkG2 are given in Table 2, calculated for the complete set of nuclei, but also for subsets of nuclei separated by the number parity of the two nucleon species. For comparison, we also list the values for the BSkG1 model obtained through identical calculations but for the usage of the Equal-Filling Approximation (EFA) [93] for odd-mass and odd-odd nuclei. We show in Fig. 6 the differences for individual nuclei between the empirical values and the calculations, $\delta O \equiv O^{\text{emp}} - O^{\text{th}}$, as a function of neutron (left column) and proton number (right column).

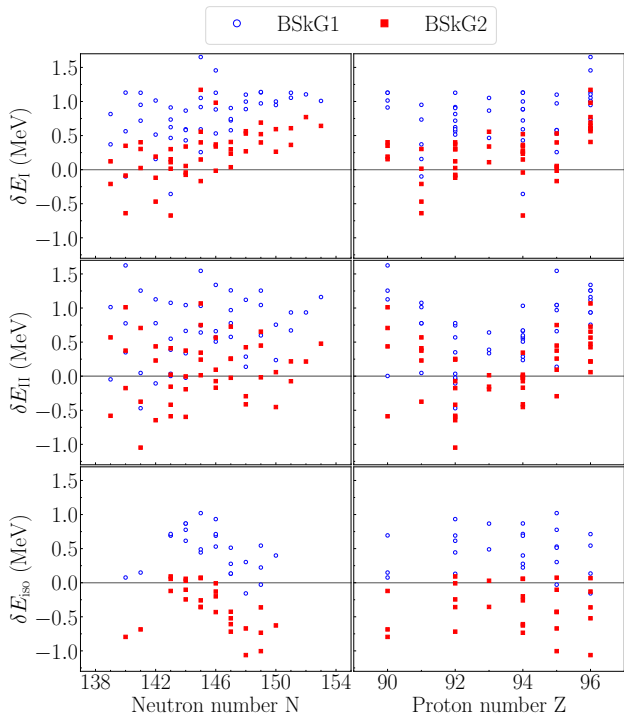


Fig. 6 (Color online) Difference between calculated and reference values for the primary barrier heights (top panel), secondary barrier heights (middle panel) and isomer excitation energies (bottom panel), using BSkG1 (blue open circles) and BSkG2 (red filled squares). Positive (negative) values for all three differences mean that calculated results are smaller (larger) than the reference values.

BSkG1 reproduces the empirical values for barriers and isomer excitation energies roughly within 1.5 MeV; the largest deviation between empirical and calculated values for primary barriers occurs for ^{241}Cm at roughly 1.6 MeV. The total rms deviations for the three quantities for BSkG1 are all slightly below 1 MeV. This level of agreement with the reference values is not typical among all Skyrme parameterizations, many of which overestimate fission barriers by as much as 10 MeV [37]. As we will see in Sec. 4.4, it is however roughly representative of the subset of models whose parameter adjustment considered fission in one way or another [71, 74]. Since the construction of BSkG1 did not involve fission properties, its quality in this respect is thus somewhat remarkable. Nevertheless, the mean deviations of this model are all larger than 0.6 MeV, indicating a systematic underestimation of inner and outer barriers as well as isomer excitation energies.

By adding the vibrational correction and adjusting to fission data, BSkG2 does significantly better than BSkG1 for the primary barriers. The total BSkG2 rms deviation for this quantity is only $\sigma(E_I) = 0.44$ MeV, which is half that of BSkG1. The BSkG2 mean deviation of the primary fission barrier is much smaller,

$\bar{\epsilon}(E_I) = +0.24$ MeV, but remains non-zero and positive. The largest difference between the empirical values and the calculations still occurs for ^{241}Cm , but this is the only nucleus whose primary barrier is not reproduced within one MeV. The reproduction of the secondary barriers is also much improved, as shown by an rms deviation of $\sigma(E_{II}) = 0.47$ MeV. The corresponding mean deviation, $\bar{\epsilon}(E_{II}) = +0.10$ MeV, is even smaller than that of the primary barriers but also indicates a small but systematic underestimation of the secondary barriers. The BSkG2 rms deviation of isomer excitation energies is less than half of its predecessor, $\sigma(E_{\text{iso}}) = 0.49$ MeV, which is as accurate as the description of the barriers. However, the model overestimates E_{iso} for nearly all nuclei we consider, which is reflected in the large *negative* mean deviation, $\bar{\epsilon}(E_{\text{iso}}) = -0.36$ MeV, in contrast to the systematic underestimation of this quantity by BSkG1. The mean and rms deviations restricted to subsets of nuclei show that these observations generally hold separately among the subsets of even-even, odd- Z , odd- N and odd-odd nuclei. One difference among subsets concerns the mean deviation of the primary barrier: for the small number of odd- Z and odd-odd systems it is smaller ($\bar{\epsilon}(E_I) = -0.03$ and $+0.13$, respectively) than that for the large number of even-even and odd-odd nuclei ($\bar{\epsilon}(E_I) = +0.31$ and $+0.34$, respectively). Despite this difference and other more minor ones, the deviations in Table 2 are comparable among all subsets, indicating that our choice to include only 12 even-even nuclei in the objective function did not bias the parameter adjustment.

The mean deviations of BSkG2 are small but non-zero: the tendency of the model to overestimate isomer excitation energies while slightly underestimating barriers can be seen in Fig. 6. This deficiency cannot be solved by further fine-tuning of the collective correction: as is clear from the discussion in Sec. 3, the parameters of E_{corr} do not offer the possibility to simultaneously *raise* the barriers and *lower* the isomer excitation energies. It is tempting to look for further trends in the deviations as a function of particle number in Fig. 6, but we remind the reader that (i) empirical values are only available for a tiny fraction of the nuclei relevant to nucleosynthesis and (ii) that the empirical values themselves are subject to uncertainties, as we remarked on in Sec. 2.3. Furthermore, the mean deviations of BSkG2 are not much larger than the numerical precision of our calculations, roughly 100 keV. One could argue that the BSkG2 mean deviation for the secondary barriers essentially vanishes, even though this quantity remains the average of much larger errors, see Fig. 6.

The accuracy of BSkG2 as reflected by the small rms and mean deviations in Table 2 is excellent com-

pared to other large-scale models of fission properties in the literature and it is striking that the rms deviation of the primary barriers, secondary barriers and isomer excitation energies are all comparable. We will discuss these observations in more detail in Sections 4.2 and 4.4, but note here already that the success of BSkG2 is not solely due to inclusion of the vibrational correction: the first step of the parameter adjustment resulted in a parameterization with fission properties similar to those of BSkG1, even though no information on the properties of nuclei at large deformation entered this phase of the fit. The quality of this intermediate parameterization for fission is not a given; instead it results from the choices made in our modelling of the nuclear binding energy such as the inclusion of the two-body part of the centre-of-mass correction. The adjustment procedure of many available Skyrme parameterizations only accounted for its one-body part, resulting in significantly larger surface tensions [52, 75] and an overestimation of fission barriers by 10 MeV or more [37] unless explicitly constraining deformation properties as done for SkM* [71] or SLy5s1 [37]. Through fine-tuning of the parameters of the collective correction, we were able to reduce the rms and mean deviations of fission properties from values comparable to those of BSkG1 to the final BSkG2 values in Table 2. We repeat here that the quality of the model for g.s. properties did not meaningfully suffer from this second step of the parameter adjustment: BSkG2 achieves an rms deviation on essentially all known nuclear masses of AME2020 [39] of $\sigma(M) = 0.678$ MeV, slightly better than that of BSkG1 and competitive with most other models in the literature [12].

To conclude this section, we confirm that the PES of all nuclei we consider here has a topography similar to those discussed in Sec. 3. In Fig. 7, we illustrate this similarity by showing the location of the saddle points and isomers in terms of the quadrupole deformations β_{20} and β_{22} , as well as the octupole deformation β_{30} . The multipole moments of all three quantities evolve slowly and smoothly with neutron number. They depend only slightly on proton number, with the exception of the isotopes with lowest Z (Th, Pa, U) whose outer barrier is somewhat different from the trend of the other isotopic chains. We point out that *all* inner and outer saddle points are located at non-zero values of β_{22} . Although the corresponding curves are not drawn in Fig. 7, all ground state and isomeric minima are axial and reflection-symmetric, meaning that for those features of the PESes $\beta_{22} = \beta_{30} = 0$. Although this cannot be deduced from the tables and figures shown so far, the superdeformed minimum is always higher in energy than the g.s. minimum near $\beta_{20} \sim 0.3$: E_{iso} is posi-

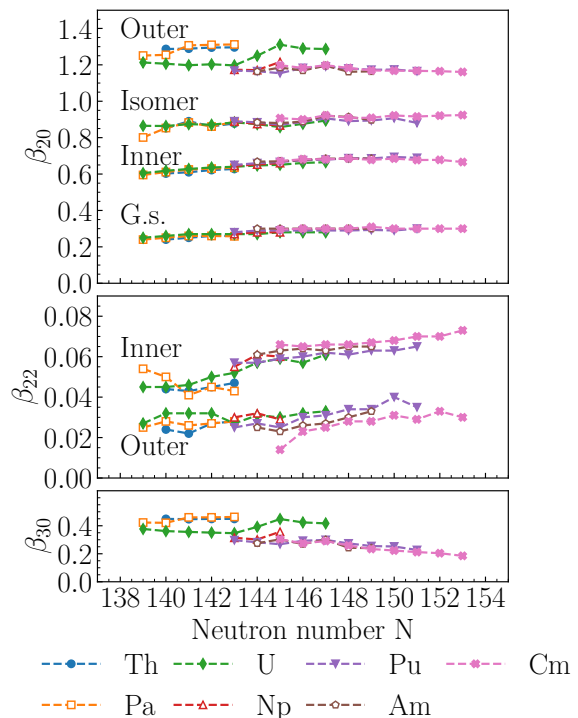


Fig. 7 (Color online) Calculated quadrupole deformations β_{20} (top panel) and β_{22} (middle panel) as well as octupole deformation (β_{30} , bottom panel) for different features of the PES as a function of neutron number: the g.s. minimum, the inner saddle-point, the superdeformed isomeric minimum and the outer saddle point. Note that $\beta_{22} = \beta_{30} = 0$ for all ground states and isomers and $\beta_{30} = 0$ in all cases save for the outer saddle points; these curves are not shown. Even- Z isotopes are drawn with full symbols, odd- Z with empty symbols.

tive in all cases, even for BSkG1 which systematically underestimates this quantity.

One minor further difference separates the Th isotopes from the other nuclei: their PESes show a shallow third minimum at $\beta_{20} \sim 1.6$ and a third, barely pronounced, saddle point near $\beta_{20} \sim 2.0$ which is several MeV lower than even the secondary barrier and is thus of little consequence for our discussion. This topography is similar to those described in Refs. [72, 80], although in other calculations this outermost (third) saddle point can determine the primary barrier [57]. Exploratory calculations show that Th isotopes with $N \leq 138$, isotopes that do not figure in this study, can acquire an octupole deformation in their g.s. when calculated with BSkG2.

4.2 The impact of triaxiality

For the five examples of Sec. 3, we found that the inclusion of triaxial deformation has a large impact on inner barrier and a smaller effect on the outer barrier. In this

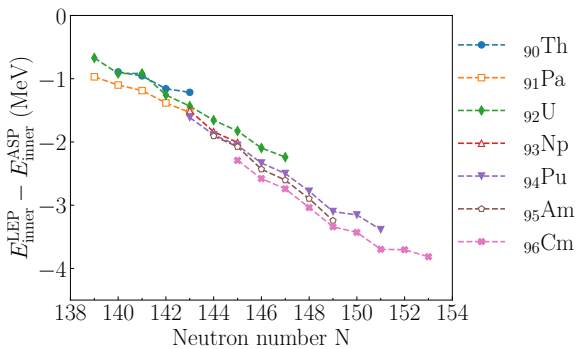


Fig. 8 (Color online) Effect of triaxial deformation on the inner fission barrier $E_{\text{inner}}^{\text{LEP}} - E_{\text{inner}}^{\text{ASP}}$, as a function of neutron number N . Isotopic chains with even Z and odd Z are drawn with full and empty symbols, respectively.

section, we investigate this effect for the complete set of nuclei and study its evolution with particle number. This section does not discuss isomer excitation energies; the corresponding mean-field configurations are all axially symmetric.

We show in Fig. 8 the energy difference between the inner barriers along the two fission paths: LEP–ASP. The difference of both barriers grows rapidly with increasing neutron number, ranging from about 650 keV for ^{231}U to slightly less than 4 MeV (^{249}Cm). This is a significant correction for nuclei with $N \sim 140$ and is an enormous change for the nuclei with $N \sim 150$, for which the empirical primary barriers are on the order of 5 MeV. Similarly, Fig. 9 shows the energy difference of the outer barriers along the LEP and the ASP. The impact of triaxial deformation on the outer barrier is more modest, but is larger than 400 keV for most of the nuclei we consider, ranging from virtually no effect for ^{240}Am to about 850 keV for ^{247}Pu . Although we do not show the corresponding curves, the energy differences obtained with BSkG1 are very similar.

A striking aspect of Fig. 8 is its regularity: the triaxial energy gain for all isotopic chains fall almost on the same curve, with (i) only little deviation from a simple linear trend and (ii) very little dependence on the proton number. The latter observation suggests that the development of triaxial deformation near the inner barrier for actinide nuclei is largely driven by the neutrons. It seems that the neutrons play a similar role near the outer barrier: within a given isotopic chain, the energy difference increases linearly with neutron number. Along an isotonic chain however, the difference between LEP and ASP decreases with increasing Z except for the Th isotopes. This suggests that triaxial deformation near the outer barrier is more of a competition between neutron and proton shell effects.

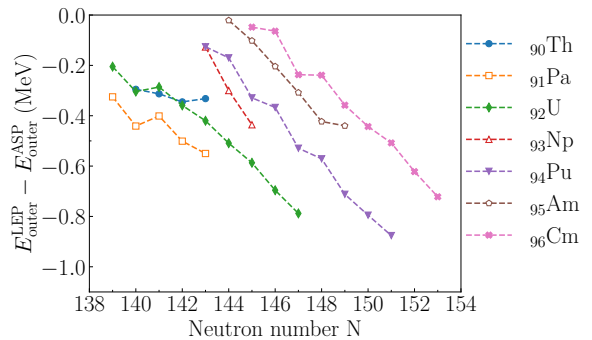


Fig. 9 (Color online) Same as Fig. 8, but for the outer barrier.

The effect of triaxial deformation is large, particularly for the inner barrier. However, it is not a priori clear that including triaxial deformation necessarily leads to an improved quantitative description of fission properties in a framework like ours, which is equipped with a collective correction whose parameters are adjusted to fission data. To clearly understand the added value of including triaxial deformation at significant computational cost, we study how well BSkG2 reproduces *differences* of fission properties:

$$\delta E_{\text{I,II}} = E_{\text{I}}^{\text{calc}} - E_{\text{II}}^{\text{calc}} - (E_{\text{I}}^{\text{emp}} - E_{\text{II}}^{\text{emp}}), \quad (8a)$$

$$\delta E_{\text{I,iso}} = E_{\text{I}}^{\text{calc}} - E_{\text{iso}}^{\text{calc}} - (E_{\text{I}}^{\text{emp}} - E_{\text{iso}}^{\text{emp}}). \quad (8b)$$

Since triaxial deformation impacts all three fission properties we consider differently, these differences emphasise the role of triaxiality. We show both $\delta E_{\text{I,II}}$ and $\delta E_{\text{I,iso}}$ in the two panels of Fig. 10: values obtained from a complete calculation with BSkG2 and those obtained from the ASP, labelled as BSkG2_{ax}. The full BSkG2 calculation with triaxial deformation describes the difference of fission barriers with high accuracy but somewhat overestimates the difference between primary barrier and isomer excitation energies. Without triaxial deformation, the differences between (i) primary and secondary barrier and (ii) primary barrier and isomer excitation energy are enormously overestimated by the model and a spurious trend with mass number can be seen for the former.

It is not possible to correct the deficiencies of the axially symmetric calculation shown in Fig. 10 by further adjustments of the parameters of the collective correction. First off, the definitions in Eqs. (8a) and (8b) essentially eliminate the influence of the vibrational correction which affects both barriers and the isomer in a roughly equal fashion. Second, changing the size of the rotational correction can alleviate the effect: for smaller values of b the difference between primary and secondary barrier will grow larger for the lighter nuclei

and smaller for the heavier nuclei in Fig. 10.⁶ To bring $\delta E_{I,II}$ close to zero for the heavy nuclei however, one would have to resort to unreasonably small and possibly even negative values of b .

We cannot exclude that changing other aspects of the model (such as the surface energy) would not result in a better description of the difference of barriers in axially symmetric calculations. As illustration, we also include in Fig. 10 results for BSk14: this model includes a rotational correction and vibrational correction adjusted in a similar fashion as those of BSkG2 but did not allow for triaxial deformation [35]⁷. BSk14 does significantly better than the axial calculations with BSkG2 but still overestimates the difference between primary and secondary barrier, particularly for the lightest and heaviest nuclei. As we will see in Sec. 4.4, the systematic overestimation of $\delta E_{I,II}$ is a generic feature of models that do not account for triaxial deformation. This is reflected in the average values of $\delta E_{I,II}$: it exceeds 1 MeV for axial calculations with BSkG2 and is about +0.46 MeV for BSk14, while the BSkG2 value of -0.14 MeV is a few times smaller.

The curves in Figs. 8 and 9 suggest that the effect of triaxial deformation grows even larger for more neutron-rich nuclei for which empirical values are not available. Since the appearance of triaxial deformation is linked to shell effects, it is unlikely that the effect of triaxial deformation across larger ranges of neutron and proton numbers will be as regular. Nevertheless, the role of triaxial deformation is not unique to the actinide region: for many superheavy nuclei it is found that triaxiality lowers the fission barrier by several MeV in both EDF-based and non-self-consistent models [44, 46, 47, 95, 96]. We are currently extending the calculations presented here to thousands of heavy and superheavy nuclei far from stability, as a significant lowering of their fission barriers compared to earlier calculations has the potential to strongly modify the role of fission in r-process nucleosynthesis.

Triaxial deformation is somewhat routinely accounted for in EDF-based studies of the inner barrier of limited numbers of actinide nuclei. We cite for instance Refs. [33, 54, 81, 82, 86, 87] which all report an effect of about 2 MeV on the inner barrier of ^{240}Pu using a va-

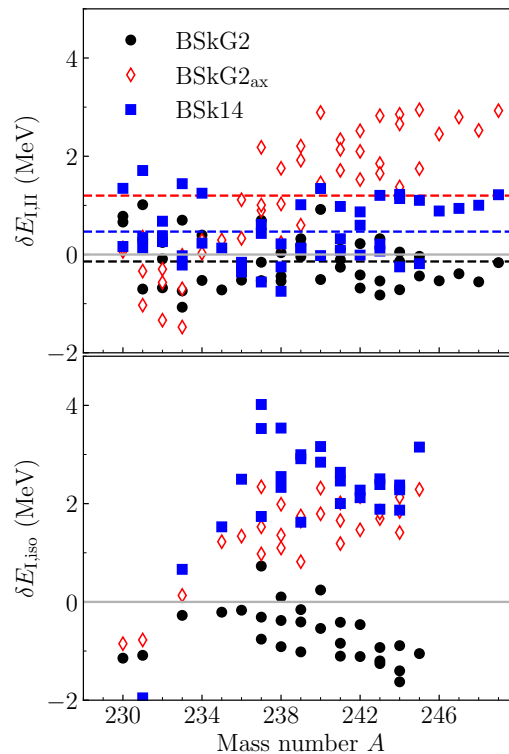


Fig. 10 Differences of fission properties $\delta E_{I,II}$ (top panel) and $\delta E_{I,iso}$ (bottom panel) for BSkG2 (black circles) and BSk14 (blue squares). We also show results constrained to axial symmetry for BSkG2 (empty red diamonds). The horizontal dashed lines in the top panel indicate the average deviation in each case.

riety of Skyrme parameterizations. A more systematic study found effects on the inner barriers of even-even actinide nuclei that are comparable to the ones we report [45]. For EDFs of the Gogny type, allowing for triaxial deformation results in a lowering of the inner barrier by about 2 MeV for ^{240}Pu [41] and up to 4 MeV for other actinide nuclei [97]. Two systematic studies employing relativistic models reported effects on the inner barrier up to about 4 MeV [42, 98].

The study of triaxial deformation near the outer barrier in EDF-based models is more recent. The relevance of shapes combining octupole and triaxial deformation for actinide fission barriers was first pointed out in the context of relativistic models in Refs. [43, 98]. The authors report energy gains due to triaxiality that grow with neutron number in the range of 0.5 to 1 MeV, i. e. slightly larger than those shown in Fig. 9. For Skyrme-type EDFs, triaxial deformation near the outer barrier was reported on for ^{240}Pu in Ref. [44] and studied more systematically for even-even actinides in Ref. [45]. The authors of the latter employ the UNEDF1 parameterization and find energy gains due to triaxial deformation that grow with neutron number and are on the order of a few hundred keV, i. e. similar in size to those we

⁶An increase of the rotational correction lowers the outer barrier more than the inner barrier, see the discussion around Fig. 5. For the heavier nuclei, the inner one tends to be the primary barrier such that an increase of b implies a larger difference between primary and secondary barriers. For the lighter nuclei, the opposite happens.

⁷We also note that both models were constructed with rather different numerical schemes: BSk14 relied on an expansion in a limited number of harmonic oscillator shells while we rely here on a coordinate space representation.

report on here. To the best of our knowledge, the possibility of triaxial deformation near the outer barrier has not yet been studied for Gogny-type EDFs.

EDF-based approaches thus paint a rather consistent picture with respect to the role of triaxiality for the barriers of actinide nuclei when constructing the LEP: up to several MeV for the inner barrier and up to one MeV for the outer barrier, both effects growing with neutron number. Triaxial deformation seems to be less important for non-self-consistent approaches: the lowering of the inner barrier for actinide nuclei due to triaxial deformation predicted by such models is typically less than one MeV [95, 99–104]. Ref. [104] is the only mic-mac study of the outer barrier that considers triaxial deformation that we are aware of: its authors report an effect of 150 keV on the outer barrier due to triaxiality for ^{248}Cm , but did not consider any other nuclei. The reduced importance of triaxiality in mic-mac models seems consistent with the observation that the gains in g.s. binding energy due to triaxial deformation in such models also tend to be smaller than in EDF-based approaches [11].

We remind the reader that our study concerns only static aspects of the fission of actinides. A more complete calculation that accounts for dynamical aspects of fission would substitute a LAP for each LEP we discuss here. The results of such a study would likely depend on (i) the treatment of the collective inertia and (ii) the selection of collective coordinates. For instance, a perturbative treatment of the collective inertia favors an axially symmetric LAP near the inner saddle point while the LAP obtained with the so-called cranking approximation for the inertia tensor is close to the LEP [105]. On the other hand, even with this approximation, the inclusion of pairing fluctuations again restores axial symmetry along the LAP near the inner saddle point [54]. However, these conclusions are so far limited in scope: they have only been established for the case of ^{240}Pu and the SkM* parameterization, and only for the inner saddle point. Furthermore, they are certainly sensitive to the details of the treatment of pairing correlations and could perhaps change when more complete treatments of the collective inertia are used [106]. More work is clearly necessary to extend these studies by (i) including outer saddle points, (ii) studying more nuclei, particularly those where the effect of triaxial deformation on the barriers is larger than for ^{240}Pu ; and (iii) improving the treatment of the inertia tensor beyond the cranking approximation.

4.3 Impact of time-reversal symmetry breaking

In order to study the impact of time-reversal symmetry breaking, we also performed a full set of fission calculations for BSkG2 with the EFA [93]. As explained in Ref. [12], treating odd-mass or odd-odd nuclei this way allows for simplified calculations yet includes the blocking effect of the odd particle(s), neglecting only the influence of the time-odd terms in the EDF. Fig. 11 shows the difference between a full calculation that accounts for the time-odd terms and one employing the EFA for all three fission properties of the 31 $Z \geq 90$ odd-mass and odd-odd nuclei in our sample. In all panels, positive (negative) values of δE_X indicates that the full calculation produces larger (smaller) values of E_X than an EFA calculation.

The barriers of odd- N , even- Z nuclei are almost entirely unaffected by the presence of time-odd terms, but the barriers of most systems with an odd number of protons get somewhat lowered. The situation is less clear for the isomer excitation energies, which can get lowered or enhanced by the time-odd terms. On the whole however, the effect of the time-odd terms is small: the largest effect in our set of nuclei is the lowering of the secondary barrier of ^{243}Am by about 220 keV while the typical effect is below 100 keV for almost all other nuclei. Although this could not have been predicted with certainty from our previous study [12], the overall small effect of time-odd terms on fission is natural in light of their limited effect on the binding energies of heavy nuclei. These results compare rather well with the more limited study of Ref. [62] for ^{239}Pu and ^{241}Pu : the authors also find a lowering of the inner barrier by a few hundred keV and a less systematic effect on the isomer excitation energies. These energy differences play almost no role in the deviations w.r.t. the empirical values reported in Table 2: when calculated with the EFA, the rms deviations on the primary barriers are 0.42 MeV, 0.51 MeV and 0.27 MeV for odd- Z , odd- N and odd-odd nuclei respectively.

The chief conclusion of this section is that the impact of time-odd terms on the fission properties of odd-mass and odd-odd nuclei is on the order of 100 keV. This is a small effect when compared to the typical accuracy of BSkG2 with respect to the empirical values and is particularly negligible when considering the conceptual problems surrounding the determination of barriers for odd-mass and odd-odd nuclei we raised in Sec. 2.2. In addition, for many nuclei the size of the effect is comparable to the numerical accuracy of our calculations, see Sec. 2.4. For these reasons, we refrain from any deeper investigation. However, the limited effect of time-odd terms on *static* properties does not mean that time-

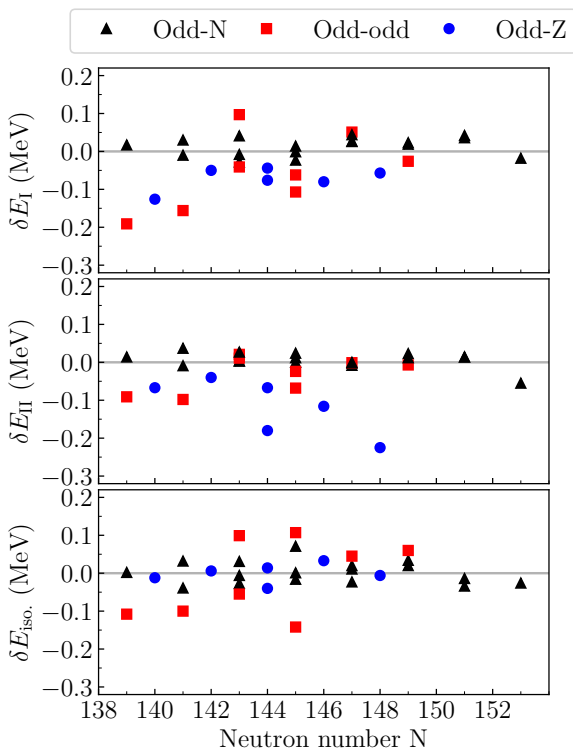


Fig. 11 The differences of fission properties obtained from an EFA calculation and a full calculation with BSkG2 ($\delta E_X = E_X^{\text{Full}} - E_X^{\text{EFA}}$) for odd-mass and odd-odd nuclei. From top to bottom: primary barriers, secondary barriers and isomer excitation energies.

reversal symmetry breaking is not relevant to nuclear fission: time-odd terms strongly affect the *dynamic* fission properties of all nuclei, including even-even ones. They appear naturally in the calculations of the collective inertia [107–109], although their contribution is omitted in the majority of studies published so far.

4.4 Comparison to other models

We have compiled in Table 3 the rms and mean deviations with respect to the empirical values for the barriers and isomer excitation energies for different models available in the literature. The first group contains all models that cover the full extent of all 45 nuclei with $Z \geq 90$ in the RIPL-3 database. This group contains four EDF-based models: BSkG1, BSkG2, BSk14 [35] and BCPM [106]. It also includes three non-self-consistent models: the ETFSI calculations based on the SkSC4 interaction [31] and the mic-mac FRLDM [103] and YPE+WS [110, 113] models. FRLDM and YPE+WS both employ a very similar Yukawa-plus-exponential (YPE) macroscopic part, but combine it with different microscopic ingredients: a Folded-Yukawa model for the former and a Woods-Saxon (WS) model for the latter.

The second and third groups consist of models whose predictions cover at least 7 even-even nuclei out of 14 in the original selection. Compared to global models, there are much more works discussing the fission properties of a limited amount of even-even actinide nuclei, such that we have limited ourselves to EDF-based models. The second group consists of non-relativistic models: Gogny-type D1M [57] and Skyrme-type UNEDF1 [45, 73], SkI3 [81], SkI4 [81], SLy6 [81] and SkM* [73]⁸. Although the calculations in Ref. [111] were extensive, they concern only even-even nuclei such that we are forced to include their Skyrme results for the SkI3, SLy6, SV-bas and SV-min parameterizations in this second group. The third group consists of relativistic models: NL-Z2 [81], NL3 [81], PC-PK1 [43] and the set DD-ME2, DD-PC1 and NL3* of Ref. [112]. NL3 and NL3* are closely related, the latter is a more modern refit of the original [114, 115]. For some data sets, isomer excitation energies or secondary barrier heights were not available.

In four cases, we list two different sets of predictions: for UNEDF1 we show the values obtained in Ref. [45] which considered triaxial deformation near both saddle points and the values of the original paper [73] which considered triaxiality only near the first saddle point. For PC-PK1, we include the complete results of Ref. [43]: the calculations limited to axial symmetry and those considering triaxial deformation. For SkI3 and SLy6 we include the results of both Ref. [81] and the more recent Ref. [111]: the results of the latter cover more nuclei, but for the former data on secondary barriers and isomer excitation energies were also available.

Table 3 also notes which models allowed for triaxial deformation: BSkG1 and BSkG2 are the only EDF-based models in the first group that account for it near both saddle points, while the mic-mac FRLDM and YPE+WS models include its effect only near the inner barrier. Several models in the second and third groups considered triaxial deformation near the inner barrier, but only two (PC-PK1 and UNEDF1) incorporated it near the second barrier. All models in Table 3 account for octupole deformation near the outer saddle point since its effect on the outer barrier is so large for actinide nuclei. For further details of the strong points and flaws of each model, we refer the readers to the original references.

The second column of Table 3 shows whether or not the parameter adjustment of the model included, in one form or another, the physics of large deformation. For the Skyrme models BSkG2, BSk14, UNEDF1

⁸Other sets of fission data obtained with SkM* exist, such as Ref. [82], but Ref. [73] reports the most extensive data set that we are aware of.

Model	Fit	Triaxial		N_b	N_{iso}	E_I		E_{II}		E_{iso}		$(E_I - E_{II})$		Ref.
		I	O			σ	$\bar{\epsilon}$	σ	$\bar{\epsilon}$	σ	$\bar{\epsilon}$	σ	$\bar{\epsilon}$	
BSkG1	N	Y	Y	45	28	0.88	+0.80	0.87	+0.71	1.00	+0.67	0.56	+0.09	
BSkG2	Y	Y	Y	45	28	0.44	+0.24	0.47	+0.10	0.49	-0.36	0.53	+0.14	
BSk14	Y	N	N	45	28	0.60	-0.27	0.69	+0.20	1.05	+0.34	0.76	-0.47	[35]
BCPM	N	N	N	45	28	1.42	-1.07	0.72	-0.30	0.52	+0.09	1.22	-0.77	[106]
SkSC4	N	N	N	45	0	0.57	+0.04	2.03	+1.78	-	-	2.15	-1.74	[31]
FRLDM	Y	Y	N	45	28	0.81	+0.22	1.41	+0.66	1.02	-0.91	0.88	-0.44	[103]
YPE+WS	Y	Y	N	45	28	0.82	-0.66	0.84	-0.40	0.38	+0.07	0.72	-0.26	[110]
D1M	Y	Y	N	14	8	0.53	+0.23	0.43	+0.06	0.99	+0.50	0.47	+0.17	[57]
UNEDF1	Y	Y	N	10	4	0.72	-0.67	0.79	-0.41	0.16	-0.06	0.83	-0.26	[73]
	Y	Y	Y	12	8	0.71	-0.52	0.65	-0.28	0.69	-0.36	0.71	-0.24	[45]
SkM*	Y	Y	N	10	0	1.92	-1.86	1.93	-1.84	-	-	0.57	-0.01	[73]
SkI3	N	N	N	7	8	3.99	-3.59	1.59	-1.44	1.04	+0.35	2.51	-2.15	[81]
	N	N	N	14	0	3.26	-2.50	-	-	-	-	-	-	[111]
SkI4	N	N	N	7	8	4.35	-4.27	3.65	-3.49	0.95	-0.22	1.02	-0.78	[81]
SLy6	N	N	N	7	8	4.23	-3.90	2.19	-2.08	1.24	-1.28	2.24	-1.82	[81]
	N	N	N	14	0	3.89	-3.31	-	-	-	-	-	-	[111]
SV-bas	N	N	N	14	0	1.88	-1.10	-	-	-	-	-	-	[111]
SV-min	N	N	N	14	0	1.61	-0.50	-	-	-	-	-	-	[111]
NL-Z2	N	N	N	7	8	1.73	-0.93	1.28	+1.19	1.81	+1.91	2.68	-2.12	[81]
NL3	N	N	N	7	8	2.18	-1.26	1.03	+0.62	0.49	+0.39	2.73	-1.88	[81]
NL3*	N	N	N	14	0	2.16	-2.03	-	-	-	-	-	-	[112]
PC-PK1	N	N	N	14	0	1.84	-1.53	1.01	-0.60	-	-	1.43	-0.93	[43]
	N	Y	Y	14	0	0.37	+0.18	0.82	+0.13	-	-	0.73	+0.05	[43]
DD-ME2	N	N	N	14	0	3.35	-3.17	-	-	-	-	-	-	[112]
DD-PC1	N	N	N	14	0	2.45	-1.76	-	-	-	-	-	-	[112]

Table 3 Rms deviations (σ) and mean ($\bar{\epsilon}$) errors ($\delta E_X = E_X^{\text{emp}} - E_X^{\text{calc}}$) for the height of the primary (E_I) and secondary (E_{II}) barriers, the excitation energy of the isomer (E_{iso}) and the barrier difference ($E_I - E_{II}$) for various models. The second column indicate whether the models parameter adjustment included information on the physics of large deformation, in one form or another. The third and fourth column indicate whether or not the calculations considered triaxial deformation near the inner and outer barrier respectively. N_b and N_{iso} respectively refer to the number of barriers and isomers included in the calculated deviations.

and SkM*, we already discussed how this was done in Sec. 2.3. The surface properties of the D1M Gogny model were adjusted along the same lines as those of the earlier D1S [8]. The objective function of the parameters of the macroscopic energy of the FRLDM model included 31 fission barriers [6]. The YPE+WS model employs the macroscopic part of an earlier version of the FRLDM model [116], which was also adjusted to 28 barriers [5]. Although no data on fission properties directly entered the fit of any of the selected relativistic models, we note that the surface properties of DD-PC1 were carefully constrained on the masses of deformed heavy nuclei [117].

Table 3 regroups a large diversity of models with a corresponding diversity in numerical accuracy. For the numerical conditions outlined in Sec. 2.4, we estimate that our calculations reach a numerical accuracy of about 100 keV that is independent of the nuclear shape and thus applies to the inner saddle point, isomer and outer saddle point equally. The results for NL3, NL-Z2, SkI3, SkI4 and SLy6 of Ref. [81] and the SkI3, SLy6,

SV-bas and SV-min results of Ref. [111] were obtained with a coordinate-space approach similar to ours: in the case of the former their choice of mesh spacing (1 fm) leads to an accuracy that is slightly lower than ours [40]. The accuracy of both sets of results nevertheless remains independent of elongation [40]. Although we are not aware of any dedicated studies, the numerical accuracy of mic-mac approaches is likely even better as most ingredients of the macroscopic part of the energy are analytical functions of the shape parameters⁹. However, all other results in Table 3 were obtained using numerical implementations relying on an expansion in a limited number of harmonic oscillator states. The numerical accuracy of such implementations is typically dependent on deformation since the harmonic oscillator spectrum is not well suited to represent very elongated shapes. Ref. [43], for example, cites a numerical accuracy of about 150 keV and 400 keV for the inner and

⁹Only the Coulomb energy and surface energy require the numerical evaluation of an integral. Nevertheless, the numerical accuracy of these terms should be easily controllable [6].

outer barriers obtained with PC-PK1. Ref. [118] cites a similar 100 keV accuracy on the inner barriers for the conditions used in Ref. [112]. In light of this issue, we will restrict ourselves to more qualitative observations of the whole of Table 3.

Correlating the third columns of Table 3 with the seventh and eighth columns shows that models that include triaxial deformation near the inner saddle barrier systematically outperform models that do not. It is also clear, but unsurprising, that models that incorporate the physics of large deformation in their parameter adjustment typically do better than others constructed without such information: the older SkM* parameterization is the only model with an informed fit that does not reach 1 MeV accuracy on the primary barriers even when allowing for triaxial deformation near the inner saddle point. The relativistic PC-PK1 parameterization is an interesting outlier: its rms deviation for the primary barriers of 14 even-even nuclei is the lowest of all models in Table 3, yet its parameter adjustment considered only spherical nuclei [119]. If triaxial deformation is not accounted for *and* large-deformation physics is not present during parameter adjustment, the resulting self-consistent models systematically overestimate the primary barriers.

BSkG2 can be compared directly with BSk14: the latter also includes both a rotational and vibrational correction whose parameters were adjusted to fission data in a two-step procedure similar to ours. For the primary barriers, arguably the most important among the three fission properties, BSkG2 improves on the BSk14 rms deviation by about 20 percent. BSkG2 also offers rms deviations on the secondary barriers and isomer excitation energies that are, respectively, more than 30 and 50 percent lower than those of BSk14. Also worthy of discussion are the mean deviations: the BSkG2 mean deviations for E_I , E_{II} and E_{iso} are comparable in size to those of BSk14, but the difference $\delta E_{I,II}$ is much more accurately described by BSkG2, as discussed above.

Table 3 also shows that *all* models that do not include triaxial deformation systematically overestimate $E_I - E_{II}$. Including triaxial deformation near the first barrier is most important; self-consistent models that do this all achieve $|\epsilon(E_I - E_{II})| \leq 0.26$ MeV while ones that do not have mean deviations that are at least twice as large. Even BSkG1 achieves an accurate description of $E_I - E_{II}$, despite its systematic underestimation of both barriers. This indicates again that the difference ($E_I - E_{II}$) is sensitive to triaxial deformation and does not depend significantly on the treatment of the collective correction.

The most important quantity for applications remains the primary barrier. In that category, BSkG2 has

the lowest rms deviation among all models in the first group. Among the second group, only D1M and PC-PK1 (with triaxial deformation) offer similar accuracy. Several models achieve a mean deviation for E_I that is comparable to that of BSkG2, but only SkSC4 does significantly better. We could have further improved slightly the performance of BSkG2 for the barriers by fine-tuning the collective correction more, but only at the cost of our description of the isomer excitation energies. However, the philosophy of the BSkG models and the older BSk models is to describe *simultaneously* as many (pseudo-)observables as possible in order to maximise predictive power. If we also take into account the secondary barriers and fission isomers, it is clear that BSkG2 is the most accurate ‘all-round’ fission model. While there are several models that can compete with BSkG2 in any given column of Tab. 3, most of them perform significantly worse in one or more other categories. The most extreme example is SkSC4, which offers one of the smallest mean deviations on the primary barriers among all models studied here but also massively underestimates the secondary barriers. D1M essentially matches the performance of BSkG2 for barriers, but not for isomers. PC-PK1 does somewhat better for primary barriers, but somewhat worse for secondary barriers. We remind the reader that for both D1M and PC-PK1, the deviations are evaluated with respect to a much smaller set of nuclei.

Finally, a remark on the number of parameters is in order: the BSkG2 model is formulated in terms of 25 parameters, somewhat more than the 22 of BSkG1 and the 24 of BSk14. This is significantly more parameters than most other EDF-based models in Tab. 3 have; for instance PC-PK1 and D1M depend on 11 and 14 parameters, respectively. Although a smaller amount of parameters constitutes an advantage for any model, one should keep in mind that we focussed here solely on fission properties: (i) BSkG2 describes several other properties of nuclei more accurately than many of the other EDF-based models in Tab. 3 and (ii) a significant number of model parameters impact the fission properties only tangentially (e.g. the spin-orbit strengths W_0 and W'_0) or even not at all (e.g. the four parameters of the Wigner energy).

5 Conclusion and outlook

5.1 Conclusions

We have presented the fission properties of the recent BSkG2 model, focussing on the effect of triaxial deformation and the effect of time-odd terms on the barrier

heights and isomer excitation energies of the double-humped fission barrier of actinide nuclei. We presented results for all $Z \geq 90$ nuclei for which empirical barriers are available in the RIPL-3 database [38] and described in detail our calculations: they are three-dimensional and simultaneously allow for octupole deformation, time-reversal symmetry breaking and triaxial deformation. The use of a coordinate-space representation of the single-particle wave functions results in a high numerical accuracy, typically about 100 keV.

We benchmarked the lowering of the inner and outer barrier due to triaxial deformation: all 45 nuclei in our sample are affected by up to 4 MeV for the inner barrier and up to 0.8 MeV for the outer barrier. The effect grows quickly with increasing neutron number for both inner and outer barriers, suggesting the importance of neutron shell effects and motivating the extension of our results to more neutron-rich nuclei. Although the effect on the barriers is large, the fission path in terms of the nuclear shape is not much affected. Time-odd terms on the other hand do not influence much the static fission properties we discuss here; their effect on the barriers and isomer excitation energies can be of either sign, but its size is typically less than 100 keV. At the time of writing, this contribution is the largest study in the context of fission of triaxial deformation and time-odd terms separately, and is the only study to combine both.

The main conclusion is that BSkG2 achieves an excellent description of the primary and secondary barriers as well as the isomer excitation energies of actinide nuclei, reaching rms deviations for all three quantities below 500 keV. Although partially due to the inclusion of fission properties in the parameter adjustment, the inclusion of triaxial deformation was crucial to achieve this level of accuracy. In particular, the new model successfully describes the difference between the primary and secondary barriers in the actinide region; models that do not incorporate triaxial deformation systematically overestimate this quantity.

We have compared the performance of BSkG2 to a large selection of models in the literature: BSkG2 offers the best description of primary barriers among all large-scale fission models for which values for all actinide nuclei are available. With the exception of PC-PK1 [43] and D1M [57], BSkG2 also outperforms most models for which only predictions for even-even nuclei are available. However, the *combined* accuracy of BSkG2 on the primary and secondary barriers as well as the isomer excitation energies is unrivalled in the published literature.

In the preceding paper, Ref. [12], we established that BSkG2 offers both a state-of-the-art description of g.s. properties and reasonable predictions for infinite nu-

clear matter. These qualities have now been combined with an unprecedented performance with respect to actinide fission barriers, rendering the model uniquely suited to provide data to nuclear applications in general and r-process calculations in particular.

5.2 Outlook

While the present study already extensively covers the actinides with known barriers, the description of a few tens of nuclei is not our ultimate aim: what is required for r-process simulations are the fission rates and fragment yields of thousands of neutron-rich nuclei for many different fission channels. This study is the first step on the way there: without a proper reproduction of experimental data and a detailed understanding of the successes and flaws of the BSkG models, we cannot have confidence in their predictions for exotic nuclei. Getting the BSkG-series to the desired point will require at least further technical developments for the calculation of inertial masses [106, 108], saddle-point level densities [120] and fragment yields [121–123], as well as an extension of all these efforts to thousands of heavy (and mostly neutron-rich) nuclei. As discussed in Sec. 4.2 and Sec. 4.3, the details of our treatment of the collective inertia might change our conclusions on the role of triaxial deformation and time-reversal symmetry breaking.

Aside from these extensions, we see two main weak points in our description of nuclear fission. The first is conceptual and concerns the determination of the barrier of odd-mass and odd-odd nuclei: can the traditional semi-classical view of fission as large-scale motion in a limited set of collective variables be applied to such systems? More precisely, it is not clear how to construct a fission path for such nuclei that connects each blocked HFB configuration to the next in a continuous way. Nor is it clear how one should choose the relevant blocked HFB configuration. For example, how is the angular momentum in the g.s. to be treated: via the construction of several different fission paths for each value of the K quantum number as in Refs. [62, 64], even when it loses its meaning when allowing for triaxial deformation? Furthermore, is an adiabatic evolution along the PES always appropriate? Given the high level density at low energy for odd-mass and odd-odd nuclei, should one incorporate the possibility of diabatic transitions for the blocked quasiparticles? The latter is also an open, though perhaps less pressing, question for even-even systems [30].

The second weak point is imposed on us by computational considerations: our approach to collective motion and in particular the vibrational correction remains

highly phenomenological out of necessity. As we remarked already in Refs. [11] and [12], symmetry-restoration techniques should be adopted to correct the deficiencies of our symmetry-broken approach which has no access to quantum numbers. Applying such techniques to the ground states of all nuclei is a significant challenge, but incorporating them into a description of fission is even more difficult. Although some works of more limited scope exist [83, 124, 125], rotational symmetry restoration has only been applied to the fission barrier of a single even-even nucleus: ^{240}Pu [47, 126]. Pending significant further developments in this direction, microscopically motivated approximations could be devised based on, for example, replacing the Belyaev MOI in Eq. (3) by the rotational and vibrational inertia obtained from a linear-response calculation. Employing linear-response techniques would also naturally provide access to a microscopic treatment of the collective inertia that is required for the determination of the LAP [30, 127].

Acknowledgements We would like to thank A. Afanasjev, S. Giuliani and P.-G. Reinhard for providing us with additional data on their calculations for use in Sec. 4.4.: these concern Ref. [112], [106] and [111], respectively. We also thank J.-F. Lemaître for sharing his flooding code. W.R. acknowledges useful discussions with N. Schunck. This work was supported by the Fonds de la Recherche Scientifique (F.R.S.-FNRS) and the Fonds Wetenschappelijk Onderzoek-Vlaanderen (FWO) under the EOS Project nr O022818F. The present research benefited from computational resources made available on the Tier-1 supercomputer of the Fédération Wallonie-Bruxelles, infrastructure funded by the Walloon Region under the grant agreement nr 1117545. The funding for G.S. from the US DOE, Office of Science, Grant No. DE-FG02-97ER41014 is greatly appreciated. S.G. and W.R. acknowledge financial support from the F.R.S.-FNRS (Belgium). Work by M.B. has been supported by the French Agence Nationale de la Recherche under grant No. 19-CE31-0015-01 (NEW-FUN).

6 Explanation of the supplementary material

We provide `Fission_Table_BSkG2.dat` as supplementary material. It contains the fission barriers and isomer excitation energies as calculated with BSkG2 for all 45 actinide nuclei considered in the text, including their location on the PES in terms of quadrupole (β_{20}, β_{22}) and octupole deformation (β_{30}). For convenience, Table 4 contains an explanation of all the columns of the file, grouped by fission property. For all nuclei, the isomer is axially and reflection symmetric ($\beta_{22} = \beta_{30} = 0$) while the inner barrier is reflection symmetric ($\beta_{30} = 0$); the corresponding multipole moments have not been included in the table.

References

1. M. Arnould and S. Goriely, *Astronuclear Physics: A tale of the atomic nuclei in the skies*, Prog. Part. Nucl. Phys. **112**, 103766 (2020).
2. C. F. v. Weizsäcker, *Zur Theorie der Kernmassen*, Z. Phys. **96**, 431-458 (1935).
3. J. Duflo and A. P. Zuker, *Microscopic mass formulas*, Phys. Rev. C **52**, 23-27 (1995).
4. P. Möller and J.R. Nix, *Nuclear masses from a unified macroscopic-microscopic model*, At. Data Nucl. Data Tables **39**, 213 (1988).
5. P. Möller, J. R. Nix, W. D. Myers, and W. J. Swiatecki, *Nuclear Ground-State Masses and Deformations*, At. Data Nucl. Data Tables **59**, 185 (1995).
6. P. Möller, A. J. Sierk, T. Ichikawa and H. Sagawa, *Nuclear ground-state masses and deformations: FRDM(2012)*, At. Data Nucl. Data Tables, **109**, 1-204.
7. F. Tondeur, *An Energy Density Nuclear Mass Formula (I). Self-consistent calculation for spherical nuclei*, Nucl. Phys. A **303**, 185-198 (1978).
8. S. Goriely, S. Hilaire, M. Girod and S. Péru, *First Gogny-Hartree-Fock-Bogoliubov Nuclear Mass Model*, Phys. Rev. Lett. **102**, 242501 (2009).
9. S. Goriely, N. Chamel and J. M. Pearson, *Further explorations of Skyrme-Hartree-Fock-Bogoliubov mass formulas. XVI. Inclusion of self-energy effects in pairing*, Phys. Rev. C **93**, 034337 (2016).
10. D. Peña-Arteaga, S. Goriely, and N. Chamel, *Relativistic mean-field mass models*, Eur. Phys. J. A **52**, 320 (2016).
11. G. Scamps, S. Goriely, E. Olsen, M. Bender, and W. Ryssens, *Skyrme-Hartree-Fock-Bogoliubov Mass Models on a 3D Mesh: Effect of Triaxial Shape*, Eur. Phys. J. A **57**, 333 (2021).
12. W. Ryssens, G. Scamps, S. Goriely and M. Bender, *Skyrme-Hartree-Fock-Bogoliubov mass models on a 3D mesh: II. time-reversal symmetry breaking*, Eur. Phys. J. A **58**, 246 (2022).
13. E. Yüksel, D. Soydaner and H. Bahtiyar, *Nuclear binding energy predictions using neural networks: Application of the multilayer perceptron*, Int. J. Mod. Phys. E **30**, 2150017 (2021).
14. S. Gazula, J. W. Clark and H. Bohr, *Learning and prediction of nuclear stability by neural networks*, Nucl. Phys. A **540**, 1-26 (1992).
15. N. Wang and M. Liu, *Nuclear mass predictions with a radial basis function approach*, Phys. Rev. C **84**, 051303 (2011).
16. N. Wang, M. Liu, X. Wu and J. Meng, *Surface diffuseness correction in global mass formula*, Phys. Lett. B **734**, 215-219 (2014).
17. R. Utama and J. Piekarewicz, *Refining mass formulas for astrophysical applications: A Bayesian neural network approach*, Phys. Rev. C **96**, 044308 (2017).
18. L. Neufcourt, Y. Cao, W. Nazarewicz and F. Viens, *Bayesian approach to model-based extrapolation of nuclear observables*, Phys. Rev. C **98**, 034318 (2018).
19. M. Shelley and A. Pastore, *A New Mass Model for Nuclear Astrophysics: Crossing 200 keV Accuracy*, Universe, **7**, 131 (2021).
20. Z. M. Niu and H. Z. Liang, *Nuclear Mass Predictions with Machine Learning Reaching the Accuracy Required by r-Process Studies*, Phys. Rev. C **106**, L021303 (2022).
21. W. Ye, Y. Qian, and Z. Ren, *Accuracy versus Predictive Power in Nuclear Mass Tabulations*, Phys. Rev. C **106**, 024318 (2022).
22. W. A. Fowler and F. Hoyle, *Nuclear Cosmochronology*, Annals of Physics **10**, 280 (1960).

Column	Quantity	Fission property	Units	Explanation
1	Z	–	–	Proton number
2	N	–	–	Neutron number
3	E	Inner barrier	MeV	Barrier height
4	β_{20}		–	Quadrupole deformation
5	β_{22}		–	
6	E	Outer barrier	MeV	Barrier height
7	β_{20}		–	Quadrupole deformation
8	β_{22}		–	
9	β_{30}		–	Octupole deformation
10	E	Isomer	MeV	Excitation energy
11	β_{20}		–	Quadrupole deformation

Table 4 Contents of the Fission_Table_BSKG2.dat file.

23. S. Goriely and M. Arnould, *Actinides: How Well Do We Know Their Stellar Production?*, *Astron. Astrophys.* **379**, 1113 (2001).
24. S. Goriely, *The fundamental role of fission during r-process nucleosynthesis in neutron star mergers*, *Eur. Phys. J. A* **51**, 22 (2015).
25. S. Björnholm and J. E. Lynn, *The Double-Humped Fission Barrier*, *Rev. Mod. Phys.* **52**, 725 (1980).
26. H. Krappe and K. Pomorski, *Theory of Nuclear Fission*, (Springer, 2012).
27. N. Schunck and L. M. Robledo, N. Schunck and L. M. Robledo, *Microscopic theory of nuclear fission: A review*, *Rep. Prog. Phys.* **79**, 116301 (2016).
28. K.-H. Schmidt and B. Jurado, *Review on the progress in nuclear fission-experimental methods and theoretical descriptions*, *Rep. Prog. Phys.* **81**, 106301 (2018).
29. N. Schunck and D. Regnier, *Theory of nuclear fission*, *Prog. Part. Nucl. Phys.* **125**, 103963 (2022).
30. M. Bender *et al.*, *Future of nuclear fission theory*, *J. Phys. G* **47**, 113002 (2020).
31. A. Mamdouh, J. M. Pearson, M. Rayet and F. Tondeur, *Fission barriers of neutron-rich and superheavy nuclei calculated with the ETFSI method*, *Nucl. Phys. A* **679**, 337-358 (2001).
32. S. A. Giuliani and L. M. Robledo, *Fission properties of the Barcelona-Catania-Paris-Madrid energy density functional*, *Phys. Rev. C* **88**, 054325 (2013).
33. M. Bender, P.-H. Heenen and P.G. Reinhard, *Self-consistent mean-field models for nuclear structure*, *Rev. Mod. Phys.* **75**, 121 (2003).
34. W. Ryssens, *Symmetry breaking in nuclear mean-field models*, Ph.D. thesis, Université Libre de Bruxelles, 2016.
35. S. Goriely, M. Samyn, and J. M. Pearson, *Further explorations of Skyrme-Hartree-Fock-Bogoliubov mass formulas. VII. Simultaneous fits to masses and fission barriers*, *Phys. Rev. C* **75**, 064312 (2007).
36. M. Kortelainen, N. Hinohara and W. Nazarewicz, *Multipole modes in deformed nuclei within the finite amplitude method*, *Phys. Rev. C* **92**, 051302 (2015).
37. R. Jodon, M. Bender, K. Bennaceur and J. Meyer, *Constraining the surface properties of effective Skyrme interactions*, *Phys. Rev. C* **94**, 024335 (2016).
38. R. Capote *et al.*, *RIPL - Reference Input Parameter Library for Calculation of Nuclear Reactions and Nuclear Data Evaluation*, *Nucl. Data Sheets* **110**, 3107-3214 (2009).
39. M. Wang *et al.*, *The AME 2020 atomic mass evaluation*, *Chin. Phys. C* **45**, 3 (2021).
40. W. Ryssens, P.-H. Heenen and M. Bender, *Numerical accuracy of mean-field calculations in coordinate space*, *Phys. Rev. C* **92**, 064318 (2015).
41. M. Girod and B. Grammaticos, *Triaxial Hartree-Fock-Bogolyubov calculations with D1 effective interaction*, *Phys. Rev. C* **27**, 2317-2339 (1983).
42. H. Abusara, A. V. Afanasjev and P. Ring, *Fission barriers in actinides in covariant density functional theory: The role of triaxiality*, *Phys. Rev. C* **82**, 044303 (2010).
43. B. N. Lu, J. Zhao, E. G. Zhao and S. G. Zhou, *Multidimensionally-constrained relativistic mean-field models and potential-energy surfaces of actinide nuclei*, *Phys. Rev. C* **89**, 014323 (2014).
44. W. Ryssens, M. Bender, K. Bennaceur, P.-H. Heenen and J. Meyer, *Impact of the surface energy coefficient on the deformation properties of atomic nuclei as predicted by Skyrme energy density functionals*, *Phys. Rev. C* **99**, 044315 (2019).
45. C. Ling, C. Zhou, and Y. Shi, *Fission Barriers of Actinide Nuclei with Nuclear Density Functional Theory: Influence of the Triaxial Deformation*, *Eur. Phys. J. A* **56**, 180 (2020).
46. S. Cwiok, J. Dobaczewski, P.-H. Heenen, P. Magierski, and W. Nazarewicz, *Shell Structure of the Superheavy Elements*, *Nucl. Phys. A* **611**, 211 (1996).
47. M. Bender, K. Rutz, P.-G. Reinhard, J. A. Maruhn and W. Greiner, *Potential energy surfaces of superheavy nuclei*, *Phys. Rev. C* **58**, 2126-2132 (1998).
48. M. Warda, J. L. Egido, L. M. Robledo and K. Pomorski, *Self-consistent calculations of fission barriers in the Fm region*, *Phys. Rev. C* **66**, 143101 (2002).
49. H. Abusara, A.V. Afanasjev and P. Ring, *Fission barriers in covariant density functional theory: Extrapolation to superheavy nuclei*, *Phys. Rev. C* **85**, 024314 (2012).
50. F. Tondeur, S. Goriely, J. M. Pearson and M. Onsi, *Towards a Hartree-Fock mass formula*, *Phys. Rev. C* **62**, 024308 (2000).
51. S. Goriely, N. Chamel, and J. M. Pearson, *Further explorations of Skyrme-Hartree-Fock-Bogoliubov mass formulas. XIII. The 2012 atomic mass evaluation and the symmetry coefficient*, *Phys. Rev. C* **88**, 024308 (2013).
52. M. Bender, K. Rutz, P.-G. Reinhard and J. A. Maruhn, *Consequences of the center-of-mass correction in nuclear mean-field models*, *Eur. Phys. J. A* **7**, 467-478 (2000).
53. S. Goriely, M. Samyn, M. Bender and J. M. Pearson, *Further explorations of Skyrme-Hartree-Fock-Bogoliubov mass formulas. II. Role of the effective mass*, *Phys. Rev. C* **68**, 054325 (2003).
54. J. Sadhukhan, J. Dobaczewski, W. Nazarewicz, J. A. Sheikh and A. Baran, *Pairing-induced speedup of nuclear spontaneous fission*, *Phys. Rev. C* **90**, 061304 (2014).

55. M. Warda, A. Staszczak and W. Nazarewicz, *Fission modes of mercury isotopes*, Phys. Rev. C **86**, 024601 (2012).
56. A. Baran, K. Pomorski, A. Lukasiak, and A. Sobczewski, *A Dynamic Analysis of Spontaneous-Fission Half-Lives*, Nucl. Phys. A **361**, 83 (1981).
57. J. F. Lemaître, S. Goriely, S. Hilaire and N. Dubray, *Microscopic description of the fission path with the Gogny interaction*, Phys. Rev. C **98**, 024623 (2018).
58. N. Dubray and D. Regnier, *Numerical search of discontinuities in self-consistent potential energy surfaces*, Comp. Phys. Comm. **183**, 2035-2041 (2012).
59. M. Bender and W. Ryssens, in preparation.
60. S. Perez-Martin and L. M. Robledo, *Fission properties of odd-A nuclei in a mean field framework*, Int. J. Mod. Phys. E **18**, 788 (2009).
61. P.-H. Heenen, B. Bally, M. Bender, and W. Ryssens, *Beyond-Mean-Field Correlations and the Description of Superheavy Elements*, Proceedings of the Nobel Symposium on the "Chemistry and Physics of Heavy and Superheavy Elements" (NS160) held at Bäckaskog Castle, Kristianstad, Sweden, May 29 - June 3 2016. D. Rudolph, L.-I. Elding, C. Fahlander and S. Åberg [edts.], EPJ Web of Conferences **131** 02001 (2016).
62. M. H. Koh, L. Bonneau, P. Quentin, T. V. N. Hao and H. Wagiran, *Fission barriers of two odd-neutron actinide nuclei taking into account the Time-reversal symmetry breaking at the mean-field level*, Phys. Rev. C **95**, 014315 (2017).
63. Rodríguez-Guzmán and L. M. Robledo, *Microscopic description of fission in odd-mass uranium and plutonium nuclei with the Gogny energy density functional*, Eur. Phys. J. A **53**, 245 (2017).
64. N. Schunck, M. Verriere, G. Potel Aguilar, R. C. Malone, J. A. Silano, A. P. D. Ramirez, and A. P. Tonchev, *Microscopic Calculation of Fission Product Yields for Odd-Mass Nuclei*, Phys. Rev. C **107**, 044312 (2023).
65. M. Bender, K. Rutz, P.-G. Reinhard and J. A. Maruhn, *Pairing gaps from nuclear mean-field models*, Eur. Phys. J. A **8**, 59-75 (2000).
66. I. Angeli and K. P. Marinova, *Table of experimental nuclear ground state charge radii: An update*, At. Data Nucl. Data Tables **99**, 69 (2013).
67. M. Samyn, S. Goriely, M. Bender and J. M. Pearson, *Further explorations of Skyrme-Hartree-Fock-Bogoliubov mass formulas. III. Role of particle-number projection*, Phys. Rev. C **70**, 044309 (2004).
68. M. Hunyadi et al., *Excited Superdeformed $K^\pi=0^+$ Rotational Bands in β -Vibrational Fission Resonances of ^{240}Pu* , Phys. Lett. B **505**, 27 (2001).
69. B. Singh, R. Zywina, and R. B. Firestone, *Table of Superdeformed Nuclear Bands and Fission Isomers*, Nuclear Data Sheets **97**, 241 (2002).
70. J. Kantele, W. Stöfl, L. E. Ussery, D. J. Decman, E. A. Henry, R. W. Hoff, L. G. Mann, and G. L. Struble, *Observation of an E0 Isomeric Transition from the ^{238}U Shape Isomer*, Phys. Rev. Lett. **51**, 91 (1983).
71. J. Bartel, P. Quentin, M. Brack, C. Guet and H.-B. Håkansson, *Towards a better parametrisation of Skyrme-like effective forces: A critical study of the SkM force*, Nucl. Phys. A **386**, 79-100 (1982).
72. J. F. Berger, M. Girod and D. Gogny, *Constrained Hartree-Fock and beyond*, Nucl. Phys. A **502**, 85-104 (1989).
73. M. Kortelainen, J. McDonnell, W. Nazarewicz, P.-G. Reinhard, J. Sarich, N. Schunck, M. Stoitsov and S. M. Wild, *Nuclear energy density optimization: Large deformations*, Phys. Rev. C **85**, 024304 (2012).
74. M. Kortelainen, J. McDonnell, W. Nazarewicz, E. Olsen, P.-G. Reinhard, J. Sarich, N. Schunck, S. M. Wild, D. Davesne, J. Erler and A. Pastore, *Nuclear energy density optimization: Shell structure*, Phys. Rev. C **89**, 054314 (2014).
75. Ph. Da Costa, M. Bender, K. Bennaceur, J. Meyer, and W. Ryssens, in preparation.
76. P. Klüpfel, P.-G. Reinhard, T. J. Bürvenich and J. A. Maruhn, *Variations on a theme by Skyrme: A systematic study of adjustments of model parameters*, Phys. Rev. C **79**, 034310 (2009).
77. M. Kortelainen, T. Lesinski, J. Moré, W. Nazarewicz, J. Sarich, N. Schunck, M. V. Stoitsov and S. Wild, *Nuclear energy density optimization*, Phys. Rev. C **82**, 024313 (2010).
78. D. Baye and P.-H. Heenen, *Generalised meshes for quantum mechanical problems*, J. Phys. A. Math. Gen. **19**, 2041 (1986).
79. H. Flocard, P. Quentin, D. Vautherin, M. Veneroni, and A. K. Kerman, *Self-Consistent Calculation of the Fission Barrier of ^{240}Pu* , Nucl. Phys. A **231**, 176 (1974).
80. K. Rutz, J. A. Maruhn, P.-G. Reinhard and W. Greiner, *Fission barriers and asymmetric ground states in the relativistic mean-field theory*, Nucl. Phys. A **590**, 680-702 (1995).
81. T. Bürvenich, M. Bender, J. A. Maruhn and P.-G. Reinhard, *Systematics of fission barriers in superheavy elements*, Phys. Rev. C **69**, 014307 (2004).
82. L. Bonneau, P. Quentin and D. Samsøen, *Fission barriers of heavy nuclei within a microscopic approach*, Eur. Phys. J. A **21**, 391-406 (2004).
83. M. Samyn, S. Goriely and J. M. Pearson, *Further explorations of Skyrme-Hartree-Fock-Bogoliubov mass formulas. V. Extension to fission barriers*, Phys. Rev. C **72**, 044316 (2005).
84. W. Younes and D. Gogny, *Microscopic calculation of ^{240}Pu scission with a finite-range effective force*, Phys. Rev. C **80**, 054313 (2009).
85. Z. P. Li, T. Nikšić, D. Vretenar, P. Ring and J. Meng, *Relativistic energy density functionals: Low-energy collective states of ^{240}Pu and ^{166}Er* , Phys. Rev. C **81**, 064321 (2010).
86. N. Schunck, D. Duke, H. Carr and A. Knoll, *Description of induced nuclear fission with Skyrme energy functionals: Static potential energy surfaces and fission fragment properties*, Phys. Rev. C **90**, 054305 (2014).
87. W. Ryssens, M. Bender and P.-H. Heenen *Iterative approaches to the self-consistent nuclear energy density functional problem: Heavy ball dynamics and potential preconditioning*, Eur. Phys. J. A **55**, 93 (2019).
88. C. E. Bemis et al., *E2 and E4 Transition Moments and Equilibrium Deformations in the Actinide Nuclei*, Phys. Rev. C **8**, 1466 (1973).
89. J. D. Zumbro et al., *E2 and E4 Deformations in ^{232}Th and $^{239,240,242}\text{Pu}$* , Phys. Lett. B **167**, 383 (1986).
90. W. Ryssens, G. Giacalone, B. Schenke and C. Shen, *Evidence of Hexadecapole Deformation in Uranium-238 at the Relativistic Heavy Ion Collider*, accepted for publication in Phys. Rev. Lett., arXiv:2302.13617.
91. P. Ring and P. Schuck, *The Nuclear Many-Body Problem*, (Springer-Verlag, New York, 1980).
92. M. Bender, P.-H. Heenen and P. Bonche, *Microscopic study of ^{204}Pu : Mean field and beyond*, Phys. Rev. C **70**, 054304 (2004).
93. S. Perez-Martin and L. M. Robledo, *Microscopic justification of the equal filling approximation*, Phys. Rev. C **78**, 014304 (2008).
94. N. Schunck, J. Dobaczewski, J. McDonnell, J. Moré, W. Nazarewicz, J. Sarich, and M. V. Stoitsov, *One-Quasiparticle States in the Nuclear Energy Density Functional Theory*, Phys. Rev. C **81**, 024316 (2010).
95. M. Kowal, P. Jachimowicz and A. Sobczewski, *Fission barriers for even-even superheavy nuclei*, Phys. Rev. C **82**, 014303 (2010).

96. P. Jachimowicz, M. Kowal and J. Skalski, *Adiabatic fission barriers in superheavy nuclei*, Phys. Rev. C **95**, 014303 (2017).
97. J. P. Delaroche, M. Girod, H. Goutte and J. Libert, *Structure properties of even-even actinides at normal and super deformed shapes analysed using the Gogny force*, Nucl. Phys. A **771**, 103-168 (2006).
98. B.-N. Lu, E.-G. Zhao, and S.-G. Zhou, *Potential Energy Surfaces of Actinide Nuclei from a Multidimensional Constrained Covariant Density Functional Theory: Barrier Heights and Saddle Point Shapes*, Phys. Rev. C **85**, 011301 (2012).
99. V. V. Pashkevich, *The Energy of Non-Axial Deformation of Heavy Nuclei*, Nucl. Phys. A **133**, 400 (1969).
100. S. E. Larsson, I. Ragnarsson, and S. G. Nilsson, *Fission Barriers and the Inclusion of Axial Asymmetry*, Phys. Lett. B **38**, 269 (1972).
101. U. Götz, H. C. Pauli, and K. Junker, *Influence of axially asymmetric distortions on fission barriers*, Phys. Lett. B **39**, 436 (1972).
102. A. K. Dutta, J. M. Pearson and F. Tondeur, *Triaxial nuclei calculated with the extended Thomas-Fermi plus Strutinsky integral (ETFSI) method*, Phys. Rev. C **61**, 054303 (2000).
103. P. Möller, A. J. Sierk, T. Ichikawa, A. Iwamoto, R. Bengtsson, H. Uhrenholt, and S. Åberg, *Heavy-Element Fission Barriers*, Phys. Rev. C **79**, 064304 (2009).
104. P. Jachimowicz, M. Kowal and J. Skalski, *Secondary fission barriers in even-even actinide nuclei*, Phys. Rev. C **85**, 034305 (2012).
105. J. Sadhukhan, K. Mazurek, A. Baran, J. Dobaczewski, W. Nazarewicz, and J. A. Sheikh, *Spontaneous Fission Lifetimes from the Minimization of Self-Consistent Collective Action*, Phys. Rev. C **88**, 064314 (2013).
106. S. A. Giuliani, G. Martínez-Pinedo and L. M. Robledo, *Fission properties of superheavy nuclei for r-process calculations*, Phys. Rev. C **97**, 034323 (2018).
107. K. Matsuyanagi, M. Matsuo, T. Nakatsukasa, N. Hinohara, and K. Sato, *Open Problems in the Microscopic Theory of Large-Amplitude Collective Motion*, J. Phys. G: Nucl. Part. Phys. **37**, 064018 (2010).
108. A. Baran, J. A. Sheikh, J. Dobaczewski, W. Nazarewicz and A. Staszczak, *Quadrupole collective inertia in nuclear fission: Cranking approximation*, Phys. Rev. C **84**, 054321 (2011).
109. K. Washiyama, N. Hinohara, and T. Nakatsukasa, *Finite-amplitude method for collective inertia in spontaneous fission*, Phys. Rev. C **103**, 014306 (2021).
110. P. Jachimowicz, M. Kowal, and J. Skalski, *Static Fission Properties of Actinide Nuclei*, Phys. Rev. C **101**, 014311 (2020).
111. J. Erler, K. Langanke, H. P. Loens, G. Martínez-Pinedo, and P.-G. Reinhard, *Fission Properties for r-process Nuclei*, Phys. Rev. C **85**, 025802 (2012).
112. A. Taninah, S. E. Agbemava, and A. V. Afanasjev, *Covariant Density Functional Theory Input for r -Process Simulations in Actinides and Superheavy Nuclei: The Ground State and Fission Properties*, Phys. Rev. C **102**, 054330 (2020).
113. P. Jachimowicz, M. Kowal, and J. Skalski, *Properties of Heaviest Nuclei with $98 \leq Z \leq 126$ and $134 \leq N \leq 192$* , Atomic Data and Nuclear Data Tables **138**, 101393 (2021).
114. G. A. Lalazissis, J. König, and P. Ring, *New Parametrization for the Lagrangian Density of Relativistic Mean Field Theory*, Phys. Rev. C **55**, 540 (1997).
115. G. A. Lalazissis, S. Karatzikos, R. Fossion, D. P. Arteaga, A. V. Afanasjev, and P. Ring, *The Effective Force NL3 Revisited*, Phys. Lett. B **671**, 36 (2009).
116. I. Muntian, Z. Patyk, and A. Sobiczewski, *Sensitivity of Calculated Properties of Superheavy Nuclei to Various Changes*, Acta Physica Polonica B **32**, 691 (2001).
117. T. Nikšić, D. Vretenar, and P. Ring, *Relativistic Nuclear Energy Density Functionals: Adjusting Parameters to Binding Energies*, Phys. Rev. C **78**, 034318 (2008).
118. S. Karatzikos, A. V. Afanasjev, G. A. Lalazissis, and P. Ring, *The Fission Barriers in Actinides and Superheavy Nuclei in Covariant Density Functional Theory*, Phys. Lett. B **689**, 72 (2010).
119. P. W. Zhao, Z. P. Li, J. M. Yao, and J. Meng, *New Parametrization for the Nuclear Covariant Energy Density Functional with a Point-Coupling Interaction*, Phys. Rev. C **82**, 054319 (2010).
120. S. Goriely, S. Hilaire and A. J. Koning, *Improved Microscopic Nuclear Level Densities within the Hartree-Fock-Bogoliubov plus Combinatorial Method*, Phys. Rev. C **78**, 064307 (2008).
121. K.-H. Schmidt, B. Jurado, C. Amouroux, and C. Schmitt, *General Description of Fission Observables: GEF Model Code*, Nucl. Data Sheets **131**, 107 (2016).
122. J.-F. Lemaître, S. Goriely, S. Hilaire, and J.-L. Sida, *Fully Microscopic Scission-Point Model to Predict Fission Fragment Observables*, Phys. Rev. C **99**, 034612 (2019).
123. J.-F. Lemaître, S. Goriely, A. Bauswein, and H.-T. Janka, *Fission Fragment Distributions and Their Impact on the r-Process Nucleosynthesis in Neutron Star Mergers*, Phys. Rev. C **103**, 025806 (2021).
124. T. V. N. Hao, P. Quentin and L. Bonneau, *Parity restoration in the highly truncated diagonalization approach: Application to the outer fission barrier of ^{240}Pu* , Phys. Rev. C **86**, 064307 (2012).
125. R. Bernard, S. A. Giuliani, and L. M. Robledo, *Role of Dynamic Pairing Correlations in Fission Dynamics*, Phys. Rev. C **99**, 064301 (2019).
126. P. Marević and N. Schunck, *Fission of ^{240}Pu with Symmetry-Restored Density Functional Theory*, Phys. Rev. Lett. **125**, 102504 (2020).
127. J. Dobaczewski, *Density Functional Theory for Nuclear Fission – a Proposal*, arXiv:1910.03924.